Review article

Kuo Zhong, Kai Song and Koen Clays*

Hollow spheres: crucial building blocks for novel nanostructures and nanophotonics

https://doi.org/10.1515/nanoph-2017-0109
Received November 7, 2017; revised January 5, 2018; accepted January 16, 2018

Abstract: In this review, we summarize the latest developments in research specifically derived from the unique properties of hollow microspheres, in particular, hollow silica spheres with uniform shells. We focus on applications in nanosphere (colloidal) lithography and nanophotonics. The lithography from a layer of hollow spheres can result in nanorings, from a multilayer in unique nano-architecture. In nanophotonics, disordered hollow spheres can result in antireflection coatings, while ordered colloidal crystals (CCs) of hollow spheres exhibit unique refractive index enhancement upon infiltration, ideal for optical sensing. Furthermore, whispering gallery mode (WGM) inside the shell of hollow spheres has also been demonstrated to enhance light absorption to improve the performance of solar cells. These applications differ from the classical applications of hollow spheres, based only on their low density and large surface area, such as catalysis and chemical sensing. We provide a brief overview of the synthesis and self-assembly approaches of the hollow spheres. We elaborate on their unique optical features leading to defect mode lasing, optomicrofluidics, and the existence of WGMs inside shell for light management. Finally, we provide a perspective on the direction towards which future research relevant to hollow spheres might be directed.

Keywords: colloidal photonic crystals; hollow spheres; nanosphere lithography; whispering gallery mode; self-assembly; surface reflection coating; visible Mie scattering.

***Corresponding author: Koen Clays,** Department of Chemistry KU Leuven, Celestijnenlaan 200D, B-3001 Heverlee (Leuven), Belgium, e-mail: koen.clays@kuleuven.be
Kuo Zhong: Department of Chemistry KU Leuven, Celestijnenlaan 200D, B-3001 Heverlee (Leuven), Belgium
Kai Song: Laboratory of Bio-inspired Smart Interface Science, Technical Institute of Physics and Chemistry, Chinese Academy of Sciences, Beijing 100190, China

1 Introduction

Hollow colloidal spheres are a type of special functional materials that possess a large fraction of empty spaces inside, intact shells, and uniform morphologies. Due to the existence of the hollow core, the surface area of the hollow spheres is much larger, while density is significantly lower than that of their solid counterparts with the same material and size. One result is that the performance of the hollow spheres in catalysis [1–4], water treatment [5], chemical sensors [6–9], and energy storage [10] is dramatically improved. On the other hand, the features of a large fraction of space inside and thin shells endow them with the ability to not only load various substances but also change the mechanical response of materials, which can be used as imaging contrast agent [11, 12], drug delivery carriers [13–15], electrode materials [16, 17], nanoreactors [18–24], and pressure sensors [25], to name a few.

In the last few years, several excellent reviews have appeared on hollow spheres or hollow micro-nanostructures [11, 24, 26–31]. However, they focused either on the synthesis with specific materials or morphologies or on the aforementioned traditional applications such as catalysis, biomedicine, nanoreactors, energy storage, and so on. There is no review that emphasizes the applications of hollow spheres as building blocks for fabrication of novel nanostructures and nanophotonics, which are inspired by the unique features of hollow spheres – empty cores and uniform shells. The structural features of hollow spheres determine their properties, while the properties of hollow spheres determine their applications. For instance, hollow spheres with dense shells can prevent liquid from infiltrating in the cores to overcome the refractive index (RI) matching problem, resulting in enhancing RI contrast to improve system performance [32–34]. Furthermore, inside the shell of hollow spheres, whispering gallery modes (WGMs) can be generated to enhance light management [35, 36]. Moreover, the existence of air core of hollow spheres results in low effective index for tuning reflectivity [37, 38]. In this review, we devote special attention to the very recent progresses on these novel applications of the hollow spheres. Especially, emphasis will be placed on what nanostructures with

novel topologies, ordered or disordered (amorphous) self-assembled nanostructures with new functionalities can be realized based on hollow spheres as building blocks. This review starts with a brief overview of the strategies for synthesis of hollow spheres. Next, self-assembly techniques are summarized including fabricating two-dimensional (2D) or three-dimensional (3D) ordered colloidal crystals or amorphous colloidal nanostructures. Afterwards, we mainly focus on the applications of the hollow spheres in different fields such as nanosphere lithography (NSL), colloidal photonic crystals (CPCs), WGM resonators, and coating materials for tuning surface reflectivity. Finally, we will discuss the current challenges and perspectives of the applications of hollow spheres.

2 Synthesis of hollow microspheres

Motivated by the unique properties, many researchers have been devoted to the synthesis of hollow microspheres with rational design for various desired applications. Until now, three main strategies have been used for the synthesis of hollow spheres, such as hard-templating, soft-templating, and self-templating methods.

For the hard-templating approach, as shown in Figure 1, in a typical process, the templates are prepared first, in which rigid monodisperse micro-nanospheres are popularly used, such as polymer beads, silica, carbon, ceramics, or metal colloidal spheres. Desired material is then coated on the outer surface of the templates. The hollow spheres are subsequently obtained after selectively removing the templates. The empty core size of hollow spheres is determined by the size of the template, while the shell thickness is mainly determined by the coating process. SiO_2 and polymer [polystyrene (PS), poly (methyl methacrylate) (PMMA)] colloidal spheres are more often used as hard templates to fabricate monodisperse organic and inorganic hollow spheres because of their high uniformity and convenient production. Compared to polymer shell hollow spheres, inorganic hollow spheres are more common, more diverse, and more stable, which endows inorganic hollow spheres with special properties in optics, optoelectronics, magnetics, photoelectrochemistry, mechanics, and catalysis [26, 27]. The most common coating material is SiO_2 [39], because it has several versatile properties. First of all, SiO_2 is hydrophilic and negatively charged, resulting in preventing the aggregation of the colloidal spheres. Second, SiO_2 is also versatile for tuning porosity, optical transparency, biocompatibility, and mechanical stability [39, 40]. Among the core particles, polymer cores such as PS colloidal spheres are widely used due to their high monodispersity and quantity production. For instance, Xia et al. [41] used a direct coating method (Stöber method) to produce silica-coated PS core-shell spheres (PS@SiO_2) with a uniform silica shell, where it requires positively charged PS spheres to get smooth and homogeneous core-shell structures. Directly using negatively charged PS spheres cannot result in a uniform shell without modification of their surfaces [42–47]. Marlow and Deng [48] reported a modified method that can directly produce monodisperse hollow silica sphere with smooth shell using negatively charged polystyrene spheres as hard templates when tetraethyl orthosilicate (TEOS) is replaced with vinyltrimethoxysilane. Several typical monodisperse hollow spheres synthesized by hard-templating method and their feature parameters are listed in Table 1.

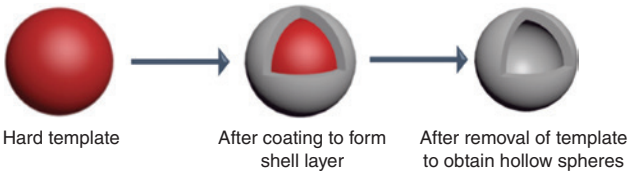

Figure 1: Schematic illustration for hard-templating synthesis process.

For the soft-templating strategy, emulsion droplets, gas bubbles, and vesicles are usually employed as templates. Although the soft-templating approach does not involve removing template process, it lacks control over the morphology and monodispersity of the products compared with the hard-templating method.

Self-templating is a direct way to synthesize hollow spheres without the need of additional templates. The advantages of the self-templating method are significantly reduced production cost, simplified synthesis procedures, and easy mass production. However, there are only several specific compositions suitable for the self-templating approach, which strictly limits its application field.

It is noteworthy that from the synthesis strategies mentioned above, only the hard-templating approach can offer hollow spheres with controllable morphology and narrow size distribution (uniformity), which can meet the strict requirements for producing ordered colloidal sphere arrays for NSL and CPCs. Further details on the state-of-the-art of synthesis of hollow spheres can be found in these reviews [26, 27, 29].

Table 1: Overview of some of hard templating methods to synthesize monodisperse hollow spheres with uniform shell.

Core type	Surface modification	Coating precursor	Shell material	Reported shell thickness (nm)	Reported diameter (nm)	Ref.
Negatively charged SiO_2	MPS	Styrene	PS	25~100	150~700	[49]
Negatively charged SiO_2	HDA	TIP	TiO_2	8~54	270~475	[50]
Positively charged PS	Not required	TEOS	SiO_2	14~90	200~950	[41, 51, 52]
Negatively charged PS	CTAB	TEOS	SiO_2	12~51	100~1500	[42, 53]
Negatively charged PS	Amine-modified	TMOS	SiO_2	6.2~17.4	95~430	[54]
Negatively charged PS	Not required	VTMS	SiO_2	33~151	284~920	[48]
Negatively charged PS	Not required	Glucose	Carbon	15~674	279~1500	[55]

CTAB, Cetyltrimethylammonium bromide; HAD, hexadecylamine; MPS, 3-(trimethoxysilyl)propylmethacrylate; PS, polystyrene; TIP, titanium isopropoxide; TEOS, tetraethyl orthosilicate; TMOS, tetramethyl orthosilica; VTMS, vinyltrimethoxysilane.

3 From colloidal spheres to colloidal arrays

Applications of the colloidal particles are strongly dependent on whether and how the colloidal particles pack. Self-assembly strategies provide a powerful tool to readily organize the colloidal spheres into ordered 2D or 3D nanostructures. Spherical nanoparticles are most often used as building blocks for the formation of high structural and optical quality colloidal crystals due to their highly isotropic features and easy stacking. To obtain high-quality colloidal crystals, the main limitation is that the colloidal spheres must be sufficiently monodisperse. Moreover, some interactions should be considered when the colloidal particles are dispersed in various solvents such as van der Waals forces, steric repulsion, and even Coulombic repulsion for charged colloids. The interactions govern both the stability of the colloids in suspension and the crystallization of the colloids, which has been demonstrated by theory and experiment [56–58]. While the assembly of colloidal spheres into ordered structures needs to meet various assembly requirements, disordered (amorphous) assembly structures can be obtained more easily as the amorphous assembled colloidal spheres do not require long-range order. We will introduce only some self-assembly strategies to produce self-assembled colloidal structures (either ordered or disordered structures) to meet the applications mentioned in this review. More details on self-assembly that cover all facts of colloidal assembly can be found elsewhere [59–62].

3.1 2D colloidal crystals

Monodisperse colloidal spheres can form a hexagonal close-packed monolayer of colloidal crystals through a number of different self-assembly methods. Several representative methods are summarized in Figure 2, including dip-coating, spin-coating, electrophoretic deposition, and interface self-assembly (Langmuir-Blodgett).

The pioneering work on fabrication of 2D colloidal crystals was developed by Nagayama et al. using dip-coating method [63], as shown in Figure 2A, in which attractive capillary forces play a key role to organize the spheres into a hexagonal monolayer close-packed array of colloidal spheres. The capillary forces result from the meniscus formed around the spheres. When the thickness of the liquid layer is very close to the diameter of the colloidal spheres, the nucleus of the colloidal crystal is generated. By continuous evaporation of the liquid, more colloids are driven towards this nucleus by a convective transport. Large-area monolayer arrays form with ordered structures via a manner of analogous epitaxial growth due to the attractive capillary forces. The quality of the obtained 2D crystals strongly relies on the evaporation rate, which is normally controlled by a step motor for lifting up the wettable substrate from the colloidal suspension with a very slow rate, or via strict control temperature for controlling the evaporation rate.

After the development of dip-coating method, spin-coating technique [64] was also proposed to accelerate solvent evaporation. The critical condition is that the substrate should be wetted completely by colloidal suspension to obtain high-quality 2D colloidal crystals (see Figure 2B). Several research groups have contributed many efforts to the spin-coating strategy to quickly produce colloidal crystals on a large scale. For example, so far, wafer-size monolayer colloidal crystals can be fabricated by spin-coating in minutes, as developed by Jiang's group [69]. Here, the colloidal spheres are spun in non-volatile solvents and are cured by UV irradiation after casting to enhance mechanical stability. This can be extended to create multilayer colloidal crystals.

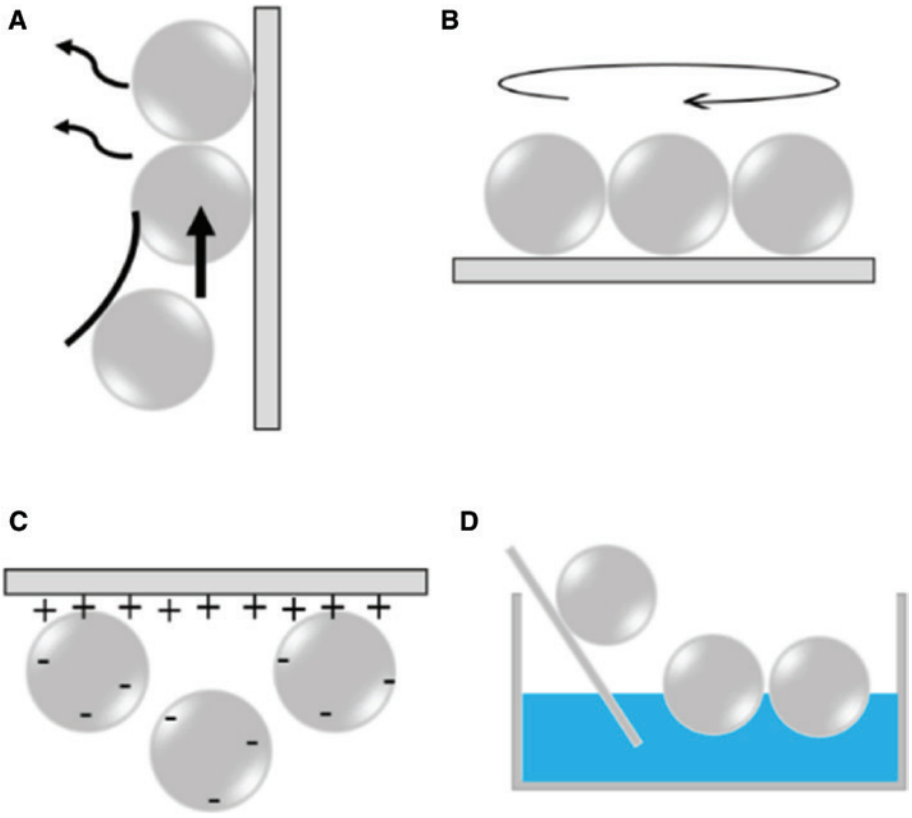

Figure 2: Various self-assembly strategies to fabricate ordered colloid arrays: (A) dip-coating [63], (B) spin-coating [64], (C) electrophoretic deposition of colloids [65, 66], (D) self-assembly at air/water interface [67, 68].

Electrophoretic deposition is an alternative method to fabricate monolayer colloidal crystals. Colloidal suspension is confined between two parallel indium tin oxide glass slides. Colloidal spheres are driven by applied electric field to form 2D colloidal arrays due to the electrohydrodynamic interaction between the spheres, as shown in Figure 2C [65, 66]. Electrophoretic deposition can also realize selective deposition on a predesigned patterned substrate and even 3D colloidal crystal [70].

Compared to the aforementioned methods, self-assembly at the gas/liquid interface (see Figure 2D) is more widely used because, for this process, no expensive equipment is needed, and colloids at the interface exclusively form a monolayer without variation in the layer thickness. In a typical procedure, a droplet of colloidal suspension is spread onto the water surface by a micropipette or needle-dripping method [67, 68], resulting in a monolayer 2D colloidal film floating on the water surface, which can subsequently be transferred onto the desired substrate. The Langmuir-Blodgett (LB) method [71–73] also belongs to the category of self-assembly at gas interface strategies, but special equipment is needed. Two hard barriers are employed to compress the floating colloidal particles to form close-packed monolayer film. In addition, binary 2D colloidal crystals can be also fabricated by the self-assembly at air/water interface [74, 75].

3.2 3D colloidal crystals

The process of colloidal spheres self-assembling into 3D ordered structures has been studied for three decades. Early theoretical calculations have demonstrated that the colloidal spheres are favored to form face-centered cubic (fcc) structures as fcc packing is slightly more stable than hexagonal close-packed (hcp) structure. However, the small difference in free energy between fcc and hcp results in the self-assembled colloidal crystals always being a mixture of these two structures [76]. A rich variety of methods have been developed to realize 3D colloidal crystals with high quality, including sedimentation, dip-coating, spin-coating, shear force driven, and vertical deposition [60, 77, 78]. Most of them are based on evaporation-driven convective assembly. Here, we will only focus on vertical deposition method (also called convective

self-assembly method) [79], which is, to date, the most widely used one to produce high-quality 3D colloidal crystals because it is low cost and large scale. During the assembly process, the evaporation of the liquid (generally, water or ethanol) drives the spheres to arrange in the meniscus formed between a vertical substrate, the suspension and air. The thickness of the colloidal crystals can be precisely controlled by adjusting the concentration of the colloidal suspension. However, this method is limited to the size of the colloidal spheres used. Normally, the diameter of the polymer spheres is larger than 1 μm, but for silica spheres, it is less than 500 nm. Recently, vertical deposition method has been successfully extended by a suitably modified method, which allows it to fabricate crystals using large spheres (diameter larger than 1 μm) [80].

3.3 Disordered (amorphous) self-assembled colloidal structures

Normally, spray coating [81, 82] or layer-by-layer [83, 84] is a commonly used approach to produce amorphous colloidal spheres with large area in a simple way. Achieving ordered self-assembled colloidal crystals requires monodispersity of the spheres and stability of the packed colloids, while for producing disordered assembled nanostructures, these criteria are not necessary.

4 From self-assembled colloidal sphere nanostructures to applications

The self-assembled colloidal structures have numerous applications in nano- and micrometer-scale materials science. For example, 2D ordered colloidal sphere arrays are usually used as masks for creating regular arrays of nanometer-sized features with a technique called colloidal (or nanosphere) lithography. Three-dimensional ordered colloidal sphere arrays are also being routinely used in the field of photonic band gap materials and sensors. While typically order is necessary for photonic structures, disordered (amorphous) colloidal sphere structures can still strongly affect light transport. In this section, we will devote special attention to the applications of hollow spheres in colloidal lithography, CPCs, visible Mie scattering for structural coloration, and tuning surface reflectivity.

4.1 Hollow nanospheres lithography

NSL, also known as colloidal lithography, uses either an individual colloidal sphere or a self-assembled monolayer or binary colloidal arrays to create (patterning) nanostructures [85]. This is an inexpensive, facile, efficient, and reproducible technique to rapidly fabricate large-area patterning nanostructures compared to conventional lithography such as electron beam lithography or focused ion beam milling [86–91]. In a typical process, close-packed colloidal sphere arrays are first prepared, serving as physical masks or templates. Nanostructures are then created through a multistep fabrication process treatment involving evaporation, deposition, imprinting, and/or etching [86, 87]. Until now, numerous nanostructures such as nanocrescents [92], nanotriangles [93], nanohoneycomb [94], nanobowl [95–97], nanorings [98–100], nanopillars [101, 102], and nanowells [103] have been achieved using colloidal spheres as building blocks. Very recently, NSL has been expanded to create more complex nanostructures by incorporating multiple-angle deposition [104], in-plane rotation etching [105], or oblique etching [106]. However, the achievements of NSL mentioned above are obtained using solid spheres as mask building blocks and involving complex fabrication processes. As compared to the solid counterparts, hollow spheres exhibit an empty core, which offers an opportunity for directly fabricating novel nanostructures when combing reactive ion etching (RIE) approach. RIE is an anisotropic etching process [107], and the morphology change of the hollow spheres is determined by the etching time. As a result, the morphology of hollow spheres can be transformed into a unique anisotropic nanostructure. In this section, we will focus on the recent efforts and developments in hollow nanosphere lithography (HNSL) for novel 2D and 3D nanostructures creation. The topic of traditional NSL based on solid spheres as building blocks is beyond the scope of this paper. Instead, we will focus on the new progress of HNSL using hollow sphere as building blocks. More details on the traditional NSL based on solid spheres can be found in other review papers [86–88, 90].

4.1.1 Direct fabrication of monodisperse nanorings from hollow spheres as building blocks using RIE

The existing traditional NSL processes still involve multiple and sophisticated fabrication steps. In addition and more importantly, they leave the created nanostructures anchored to the substrate, preventing them from being directly dispersible in an aqueous medium.

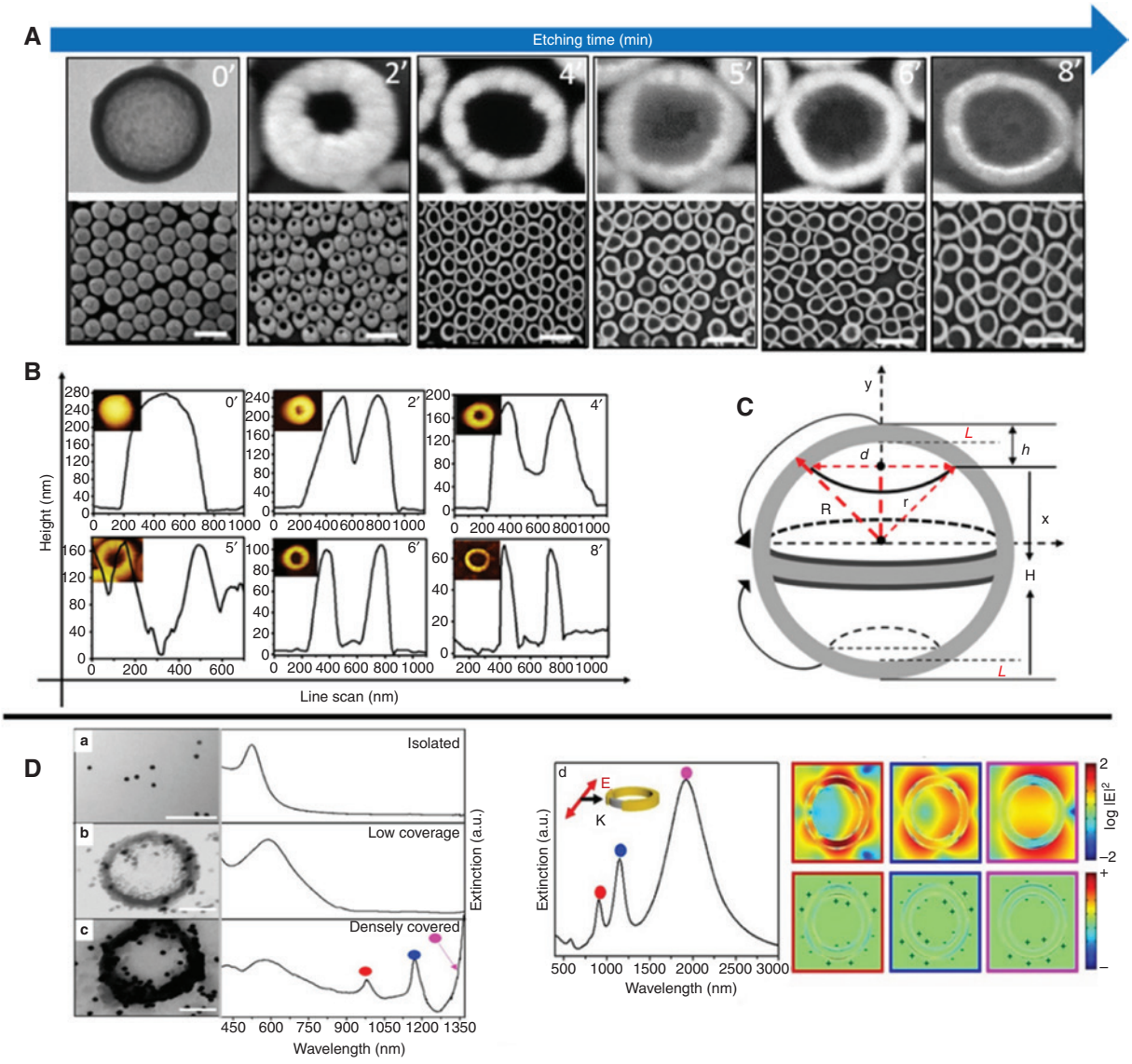

Figure 3: Direct fabrication of monodisperse silica nanorings from hollow spheres and their applications.
SEM images (A) and AFM scans (B) showing the morphology changes from a hollow silica sphere to a ring-shaped nanostructure during the etching process. All scale bars are 500 nm. (C) Schematic of the geometrical parameters used to describe the changes of the hollow spheres during the etching process. (D) Left, the optical properties of silica-Au core-shell nanorings using the obtained monodisperse silica nanorings as template. Right, simulated extinction spectra and corresponding near-filed and charge density distribution of the silica-Au core-shell nanoring composite. Adapted with permission from ref. [108], COPYRIGHT 2016 American Chemical Society.

This strongly limits the application scope and possibilities of subsequent surface functionalization. Therefore, there are still challenges for developing NSL technique to create redispersible nanostructures without involving multistep. Inspired by the empty core of hollow spheres, Zhong et al. [108] recently developed a new class of NL to directly fabricate monodisperse and dispersible silica nanorings by means of RIE of hollow SiO_2 spheres. Compared to conventional NSL, the method does not involve any intermediate steps to generate an etch mask. First, a colloidal crystal monolayer of hollow silica spheres was prepared on a substrate by assembly at the air/water interface [109]. After that, sulfur hexafluoride (SF_6) RIE etch was applied. This etching step gradually transforms the hollow silica spheres into rings. Figure 1A (SEM images) and 1B (AFM scans) shows the morphology change of the hollow silica spheres during the etching process.

As schematically illustrated in Figure 3C, the formation mechanism of the nanorings can be explained by a simple

model. The model is placed in a Cartesian coordinate system with the center of the hollow sphere as the origin and the y-axis as the etching direction. In the plasma environment, the reactive species are accelerated perpendicularly to the sample in the unidirectional electric field. This results in the top surface of the hollow spheres being preferentially etched at initial etching stage, leading to the formation of a hole on the top surface of the hollow spheres. Because of the mask effect of the sphere itself, the etching of the outside bottom surface of the hollow spheres is negligible. When the top surface is opened, the bottom surface starts being etched from the inside because the reactive species can penetrate inside the hole in the top surface of the hollow spheres. At the same time, the inside bottom surface of the hollow spheres is also being etched, resulting in formation of two holes in the top and bottom surfaces of the hollow spheres, respectively. Once there exists a hole on the bottom surface, the etching occurs at both top and bottom surfaces along the shell to the equator simultaneously, which is indicated by two arrows in Figure 3C, resulting in the morphology of the hollow spheres finally transforming into ring-shaped structures. Moreover, the resulting silica nanorings can be readily redispersed in solution and subsequently serve as universal template for the synthesis of core-shell nanoring topology. As an example, Au nanoparticles (NPs) were assembled on the silica core (nanoring) surface. By controlling the degree of Au NP coverage, the plasmonic resonance properties of the final composite nanorings can be tuned. For a dense surface coating, a novel silica-Au core-shell ring-shaped nanostructure is created, which possesses high-quality factor resonances in the near-infrared demonstrated by spectroscopic measurements and finite difference time domain simulations, as shown in Figure 3D.

4.1.2 Direct fabrication of complex 3D nanostructures from hollow sphere colloidal crystals

Tremendous efforts have been made in developing NSL, but they are still based on mono- or bilayer solid sphere colloidal array as template to create nanopatterning. The most resulting nanostructures are still (monolayer) 2D patterning, not more than two layers. This is limited by the used building blocks of solid spheres. It still remains a challenge to fabricate complex 3D nanostructures using the traditional NSL. Very recently, Zhong et al. [110] have expanded the capability of hollow sphere lithography, which allows to directly fabricate complex 3D hierarchical nanostructures based on hollow sphere colloidal crystals (HSCCs) without the need for an external mask. The obtained nanostructures have features as small as ~30 nm, which is comparable to the resolution obtained with electron-beam lithography.

The formation mechanism of these complex 3D hierarchical nanostructures can be explained by an fcc unit cell and a series of typical morphological evolutions of the hollow spheres in different layers during the etching process, as shown in Figure 4A and B, respectively. As mentioned above, during the RIE process, the reactive species are vertically accelerated to the sample surface, resulting in the top surface of the spheres being etched preferentially [108, 111, 112]. Simultaneously, the first-layer sphere array serves as shadow mask for the layer below as the reactive species can go through the interstices of the spheres. For the first layer of hollow spheres, the morphology of the spheres is transformed from hollow sphere to bowl-shaped, then ring-shaped, splitting ring-shaped, to finally form nanodot structures. For the second layer, when the top surface of the first-layer spheres is broken, triangle-shaped openings appear in the top surface of the second-layer hollow sphere at the same time due to the shadow effect from the interstices between spheres of the first layer, as described in Figure 4B (b, second). Subsequently, the triangle-shaped openings also were created on the bottom surfaces of the second-layer spheres during the bottom surfaces of the first-layer spheres broken because the reactive species can penetrate inside the hollow spheres from the broken part. However, once two holes formed on the top and bottom surfaces of the first-layer spheres, the reactive species can go through both the original triangle interstices and the broken spheres themselves of the first-layer spheres, which serve as a mask for the lower layer spheres, resulting in more complex morphologies (cage-like nanostructures) created in the second-layer spheres. Furthermore, the resulting complex nanostructures in the second layer also act as a mask for the third layer. For the third layer, what happened with the second layer is repeated, but there is a delayed etching as the etching rate decreases with increasing penetration depth for the reactive species, as illustrated in the Figure 2B, the third row. This series of structural evolution was also confirmed by SEM images in Figure 4C. Indeed, while the morphological changes in the first and second layers discussed above are already in effect, it is clear that the third layer remains unaffected (as shown in Figure 4C-2′) as the reactive species do not reach the third layer at the initial stage of etching due to the drastic reduction in flow rate of the reactive species inside colloidal crystal structures [113].

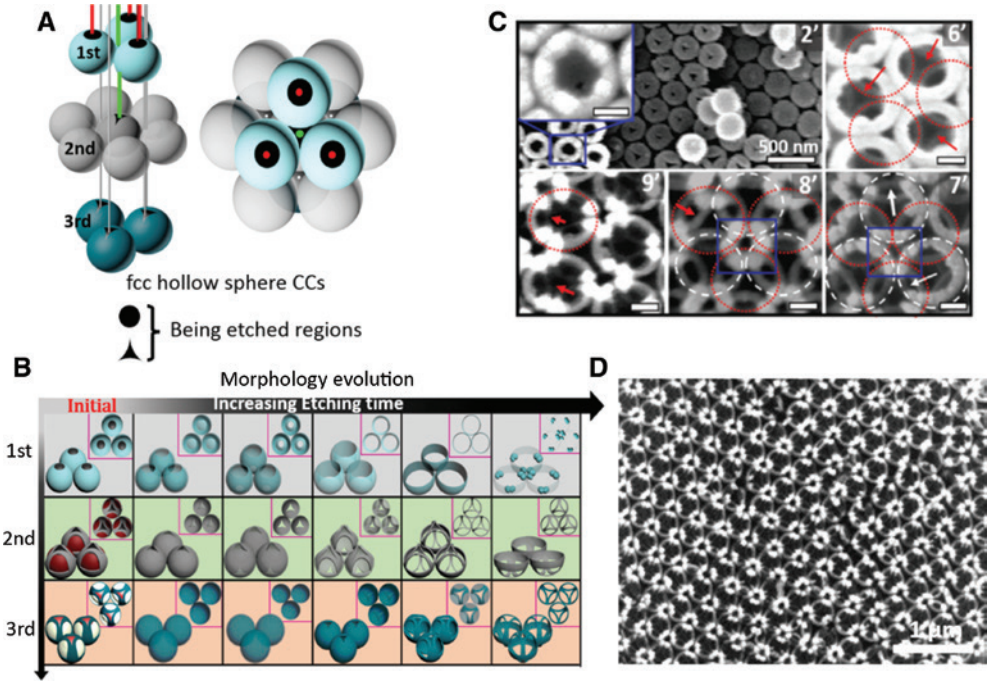

Figure 4: Direct fabrication of complex 3D hierarchical nanostructures based on hollow sphere CCs.
(A) Schematic of an fcc unit cell to illustrate the formation mechanism of the 3D hierarchical nanostructures. Black areas in the left panel of the sphere represent the etching regions, and the lines with different colors represent reactive species vertical to the (111) plane of the crystals. The right panel is the corresponding top-view. (B) Schematic of proposed mechanism for the structural evolution in HSCCs, illustrated in a layer-by-layer manner (rows) for different etching times (columns). Column a represents the initial unetched state, where black, red, and white areas denote the regions, which will be etched in the process. The colors indicate which regions will be etched simultaneously depending on the (time-dependent) shadow effect from the upper layer spheres. (C) Typical SEM images of the HSCCs during the etching process. Intermediate times of $t = 2$, 6, 7, 8, and 9 min. White and red circles indicate the first- and the second-layer hollow spheres in CCs that are not yet visible or that are already etched away, respectively. The scale bars are 100 nm. (D) An SEM image of the final complex 3D hierarchical nanostructures. Adapted with permission from ref. [110], COPYRIGHT 2016 The Royal Society of Chemistry.

4.2 Hollow spheres as building blocks for nanophotonics

Besides being templates for NSL as abovementioned, self-assembled colloidal sphere structures have another important application, normally in nanophotonics. Of course, their functionalities are strongly determined by not only the constituent materials but also the long-term, mesoscopic order (periodic or non-periodic structures). For instance, colloidal microsphere systems support strong WGM resonances that operate light in the visible range for dramatically enhancing light absorption [35, 114]. Moreover, 3D ordered colloidal crystals have been widely used in photonic crystals, termed colloidal photonic crystals or inverse opals [59–61, 77, 78, 115]. While disordered (amorphous) colloidal sphere structures are a burgeoning area in the self-assembled colloidal spheres, they herald a new era of photonic structural materials due to their wide applications in random laser [116, 117], Anderson localization [118], structural coloration [51], or anti-reflection [119]. Hollow spheres are a special case of colloidal spheres, having an empty space inside and uniform dense shell. In introducing these unique features into self-assembled hollow sphere structures, novel and fascinating properties have also emerged. In this section, we will focus on the recent progress and achievements of the self-assembled hollow spheres with ordered or disordered structures.

4.2.1 Applications of ordered self-assembled hollow sphere structures

Colloidal crystals are also called CPCs, which have been widely employed as a class of photonic crystals to manipulate light propagation in the visible range due to the existence of periodic refractive indices, forming a photonic band gap (PBG) [120]. PBG provides opportunities for modulation of optical density of states (DOS) to amplify light and matter interaction. Compared to the photonic crystals obtained by top-down approaches, CPCs are fabricated by direct bottom up self-assembly of spherical building blocks, which is low cost, scalable,

and convenient [59, 60, 78, 120]. Although various optical devices based on CPCs have been demonstrated including inhibition or enhancement of spontaneous emission [121], low-threshold lasing [122, 123], lossless waveguiding [124], and sensing [125, 126], to name a few, improving the performances and developing the novel functionalities of the CPCs are never ending. Hollow sphere CPCs (HSCPCs) provide a new avenue to further improve the performances and increase the functional diversity of the CPCs. Pioneer works on HSCPCs were reported by Asher's and Xia's groups. Asher and Xu [49] used hollow polymeric spheres as building blocks to create CPCs by self-assembly, in which the diameter and shell thickness of the hollow polymeric spheres can be tuned over a wide range by the hard-templating method. Xia et al. [41] reported HSCPCs consisting of hollow SiO_2 spheres, in which the hollow SiO_2 spheres were synthesized by Stöber method [127] using monodisperse polystyrene spheres as templates. However, they did not further study the unique properties of such CPCs, which are caused by their specific hollow features. Together with hollow polymeric spheres, a silica shell on hollow spheres is the most commonly used building blocks, due to their organic solvents resistance, thermal stability, and easy surface functionalization. Clays et al. [128] studied the optical properties of the hollow silica sphere CPCs after infiltrating different organic liquids. They further found that such a system can overcome the RI matching problem with liquid infiltrating, unlike with the traditional solid sphere CPCs or inverse opals. The dense shell of the hollow SiO_2 spheres can prevent liquid from infiltrating, leading to increasing the RI contrast. RI matching is a severe problem that limits the use of the traditional CPCs in some specific conditions such as under outdoor varying weather conditions or under aqueous environment for real-time sensing. In addition, the existence of WGMs inside the shell of hollow spheres has also been demonstrated for light management to improve the performance of optoelectronic devices. In this subsection, we will review a number of elaborations of hollow sphere CPCs, such as engineering defect modes in CPCs and defect mode lasing, patterned CPCs for real-time fluorescence detection and optomicrofluidics, selective sensing of the CPCs, robust sealed CPCs with ultrastable PBG and WGM resonators for light management.

4.2.1.1 Engineering planar defects in CPCs and defect pass mode laser

Analogous to doping in semiconductors, defect modes can be introduced into photonic crystals to create allowed states (the pass band) within the forbidden band (PBG), resulting from the DOS redistribution (enhancing the DOS) in the defect mode [129, 130]. Introducing defects into photonic crystals in a controllable manner is as important as that of dopants in semiconductors, because it can provide more functionalities for photonic crystals. For instance, waveguides with bend radii on the order of the wavelength without significant loss of signal, low-power all-optical switching, and low-threshold laser can be achieved by introducing suitable defects into photonic crystals [131, 132]. Normally, the defect modes can be created in photonic crystals by locally disrupting the periodicity or the RI of the photonic crystals [129, 130]. An interesting special defect mode for CPCs is a planar defect, because they are technically easy to create. When a planar defect is introduced in CPCs, it results in localized states in the stop band (the PBG), leading to a pronounced dip in the corresponding reflectance spectra. So far, many techniques have been developed to introduce a planer defect into CPCs, such as Langmuir-Blodgett [133–136], chemical vapor deposition [137, 138], spin-coating [139], transfer printing [140–142], and sputtering [143, 144]. However, most of the reported results are not satisfying as they cannot produce a sufficiently pronounced passband within the PBG.

Recently, Zhong et al. [109] developed a facile way that can significantly improve the quality of the introduced defect mode pass band. Typically, high-quality 2D monolayer of SiO_2 spheres (guest spheres) was first fabricated by self-assembly at the air/water interface using surfactant as "soft barrier" to compress the individual microspheres into long-range hexagonal arrays, as shown in the inset of Figure 5A. Then the floating monolayer acting as defect layer was transferred onto a prepared CPC consisting of silica-coated polystyrene spheres (PS@SiO_2 core-shell spheres, host spheres). Finally, after deposition of a second CPC of host core-shell spheres on the surface of the defect layer, sandwiched CPCs are obtained, as shown in Figure 5A. Compared to the previous methods to introduce planar defects into CPCs, this method results in much more pronounced pass bands in the PBG of the CPCs. More importantly, the full width at half maximum of the obtained pass band is only 16 nm, as can be seen in Figure 5B. To understand how the defects affect the optical properties of the sandwiched CPCs, different defect modes were obtained and studied by adjusting the size of guest spheres and/or transforming the material nature of host spheres from PS@SiO_2 core-shell spheres to hollow SiO_2 spheres by calcination, as shown in Figure 5C.

As discussed above, insertion of defect modes into PhCs in a controlled manner can provide more opportunities to diversify their applications, especially in photonic crystal lasers [145–147]. Until now, lasers based on

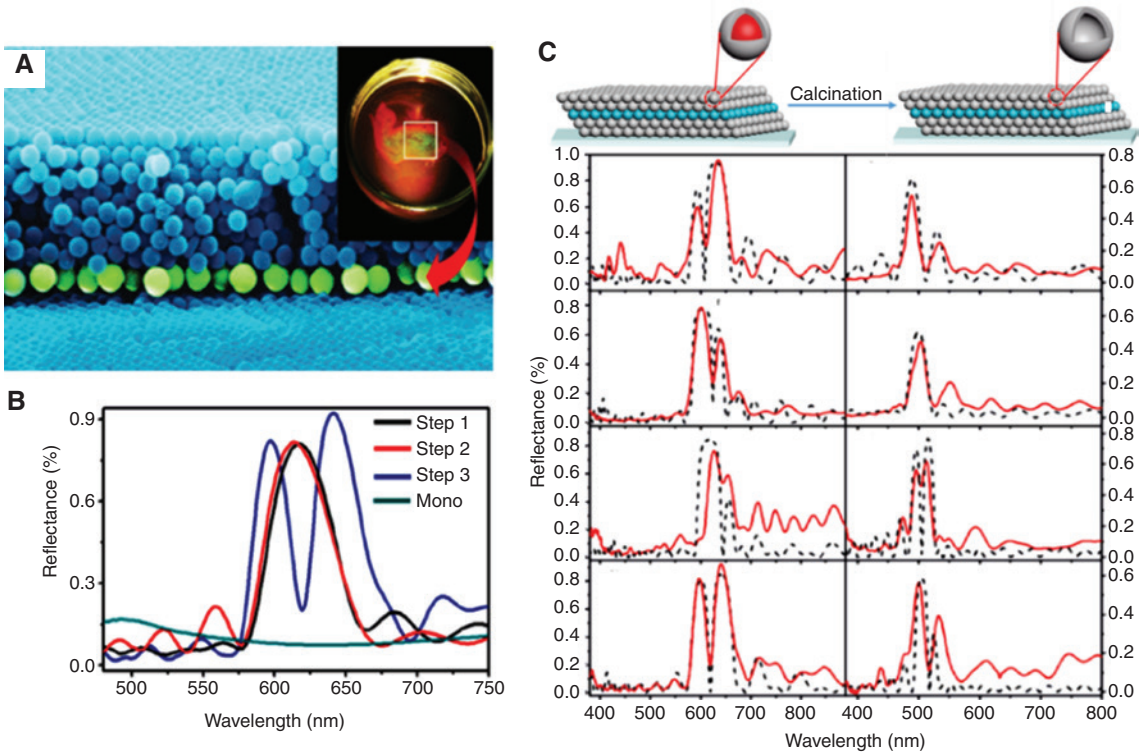

Figure 5: Introduction of a planar defect into CPCs for pronounced passband.
(A) A typical SEM image of sandwiched CPCs with a defect layer as indicated by the green color. (B) Reflectance spectra of different fabrication steps, in which steps 1, 2, and 3 represent the bottom CPC consisting of PS@SiO_2 spheres, after deposition of the defect layer on the surface of the bottom CPC, and after deposition of the second CPC, respectively. (C) Experimental (solid) and simulated (dashed) reflectance spectra from a series of sandwiched CPCs with various thicknesses of defect layer. Left column, PS@SiO_2 core-shell spheres as building blocks. Right column, hollow SiO_2 spheres as building blocks obtained after calcination. Adapted with permission from ref. [109], COPYRIGHT 2014 The Royal Society of Chemistry.

photonic crystal cavities (defect modes) have been almost exclusively demonstrated by top-down fabricated PhCs. Only a few reported results demonstrate lasing in defect mode based on bottom-up engineered CPCs, as the quality of the defect mode created by bottom-up methods is usually not good enough to allow lasing in the pass band (defect mode). Most of CPC lasers are based on the photonic band edge effect [122, 148].

Very recently, Zhong et al. [149] further experimentally and theoretically demonstrated, for the first time, lasing oscillation within the defect mode pass band of the self-assembled CPCs. The middle layer of the large spheres (guest) was modified by laser dye (Rhodamine B, RhB) to serve as a defect layer and a gain medium simultaneously, as shown in Figure 6A. A pronounced pass band with very narrow line width (~11.7 nm) is observed in the reflectance spectrum at a wavelength of ~591 nm, as shown in Figure 6B. When using low energy to excite the sample, a broad emission spectrum of RhB molecules was observed around a wavelength of 572 nm. While increasing the pump energy, a narrow peak suddenly appears at the long wavelength shoulder of the broad fluorescence spectrum when the excitation energy reached 14.3 μJ (see Figure 6C, left panel). Upon further increasing the excitation energy, the line width of the emission spectrum dramatically narrows while the amplitude is simultaneously enhanced. The narrowest line width of the emission line is 0.77 nm (see Figure 6C, right), when increasing the excitation energy. Furthermore, the simulations reveal that the relative low-threshold lasing exhibited by the sandwich structure can uniquely be attributed to the efficient coupling of the spontaneous emission of the dye to the defect mode of the doped crystals.

4.2.1.2 Patterned superhydrophobic/superhydrophilic surfaces of hollow sphere CPCs for real-time fluorescence detection

It is well known that creating superhydrophobic surfaces should combine surface roughness with low surface energy [150]. So far, there is no single chemical modification known that can produce a smooth surface with

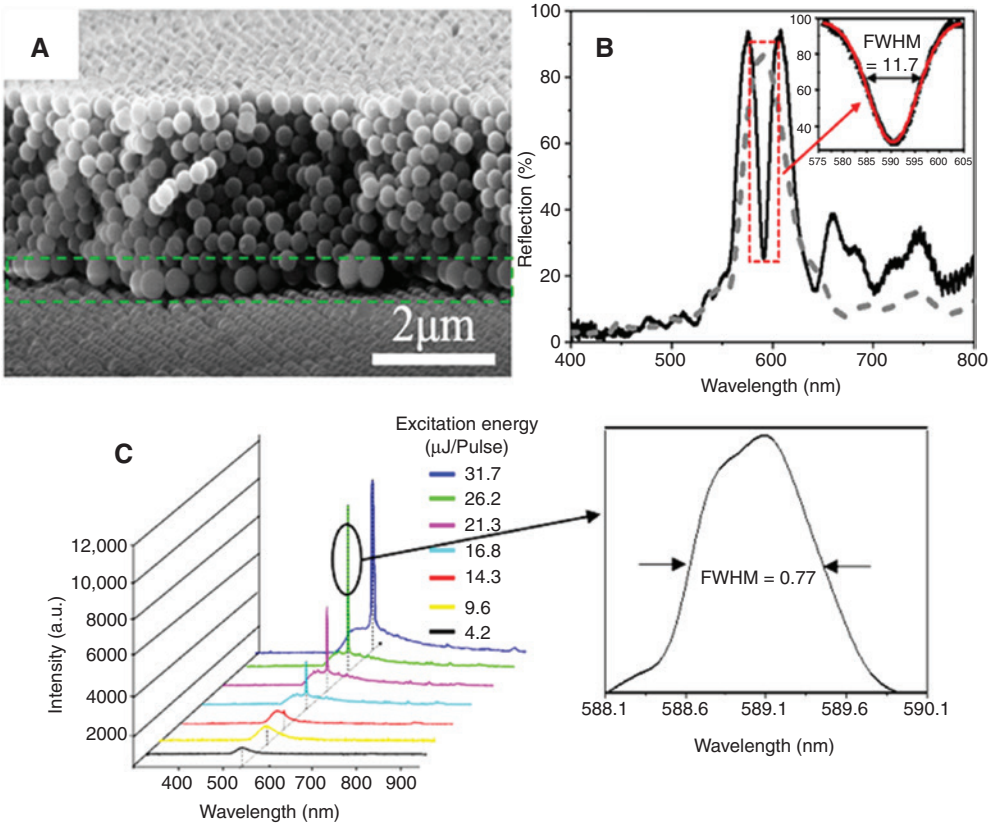

Figure 6: Defect mode passband lasing in sandwich-like CPCs.
(A) A typical SEM cross-section view of the obtained sandwiched CPCs with a defect layer as indicated by green lines. (B) The optical properties of the CPCs with (black solid line) and without (grey dashed line) a defect layer. (C) Emission spectra obtained from the sandwiched CPCs with various excitation energy. Adapted with permission from ref. [149], COPYRIGHT 2016 American Chemical Society.

superhydrophobicity. Self-assembled CPCs provide an opportunity to obtain superhydrophobic surfaces with a suitable surface modification due to their inherent surface roughness. Combing the unique optical properties of CPCs with the specific surface wettability not only broadens the application range of CPCs in various optical devices but also improves their performances [151–153]. For instance, an ultrasensitive fluorescence sensor based on hydrophilic/hydrophobic patterned CPCs has been developed by fabricating hydrophilic CPC dots on a hydrophobic substrate using the inkjet printing technique [154]. Such patterned CPCs are inspired by the hydrophilic/hydrophobic patterned back of beetle that has an ability to collect and enrich water from fog [155]. Moreover, CPCs with extremely wetting patterns have been used for microfluidics because the flow only wets and moves along the hydrophilic regions. However, these patterned CPCs are not suitable for real-time sensing as their optical properties are dramatically diminished when water penetrates the building blocks of solid colloidal spheres resulting in the RI index matching problem. How to improve the performances of the CPC devices for real-time detection is still a challenge. As mentioned above, using hollow spheres as building blocks to replace the solid colloidal spheres provides an effective way to overcome the RI matching problem. Hollow sphere CPCs show remarkable advantages and unique properties in this content.

Recently, Zhong et al. [34] developed a hollow sphere CPC system for real-time fluorescence detection in aqueous system. Because the dense shell of the hollow sphere prevents liquid from infiltrating the inner cavity, liquid can only replace the air between the microspheres but not inside. Thus, hollow sphere CPCs exhibit the ability to maintain a high RI contrast after the infiltration of water (physiological environment), leading to exceptionally strong photonic band gap effects and fluorescence enhancement, which is essential for real-time fluorescence detection in aqueous system. In addition, they introduced superhydrophilic patterns on the superhydrophobic hollow spheres CPCs, as shown in Figure 7A. Oxygen plasma etching was employed to

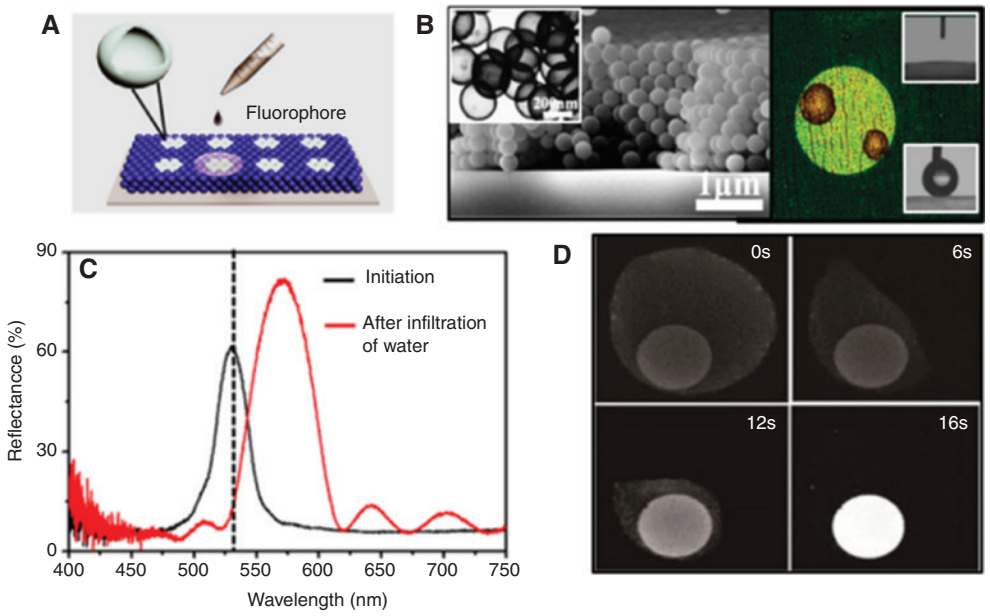

Figure 7: Fabrication of patterned HSCPCs for real-time fluorescence detection.
(A) Schematic illustration of the superhydrophobic hollow sphere CPCs with superhydrophilic patterns. (B) The structural properties of the patterned hollow sphere CPCs. (C) The optical properties of the superhydrophilic region of the patterned sample before and after infiltration of water. (D) Fluorescence images sequences of enrichment process on the patterned HSCPCs. Adapted with permission from ref. [34], COPYRIGHT 2017 American Chemical Society.

create superhydrophilic patterns on the superhydrophobic hollow sphere CPCs. The related structural properties of the hollow sphere building blocks and the patterned hollow sphere CPCs are shown in Figure 7B. Figure 7C shows the shift and amplitude enhancement of the reflectance peak of the superhydrophilic regions of HSCPCs after water infiltration. The shift is attributed to the effective RI increase, while the amplified enhancement refers to the relative RI contrast increase. After water infiltration into the voids in HSCPCs, the RI of the voids among sphere changes from 1 (air) to 1.33 (water), while that of the core of the hollow sphere still remains air (dense shell preventing water infiltration). This results in both effective indices and RI contrast increase. The patterned hydrophilic regions (pinning centers) in an otherwise hydrophobic environment were used to strongly confine and concentrate water-soluble analytes, again leading to a significant (local) increase in fluorescence, as shown in Figure 7D. The orthogonal nature of the PBG and enrichment effect allows for a multiplicative effect, resulting in an increase of fluorescence, allowing enhanced real-time fluorescence detection without any sample preparation.

Incorporation of high-performance optical devices into microfluidics has recently attracted great attention due to the emerging unique properties. Such a system is also termed optomicrofluidics, which combines the advantages of optics with microfluidics to realize rapid *in situ* sensing of analytes. CPCs in particular are promising candidates to be integrated into optomicrofluidic systems. However, the traditional CPCs always consist of solid spheres that result in an inherent RI matching problem when the voids in CPCs are filled with water. This drawback leads to significantly diminishing or even completely vanishing optical properties of CPCs. Zhong et al. [33] introduced a superhydrophilic channel into superhydrophobic HSCPCs, which form an optomicrofluidic device. This hollow-sphere-based optomicrofluidics results in stronger a PBG effect rather than in RI matching. Figure 8A shows the fabrication process. By combining simple surface modification and selective oxygen plasma etching, an integrated HSCPC optomicrofluidic systems can be achieved. A typical cross-section SEM image of HSCPCs is shown in Figure 8B. The aqueous solution is only penetrating the superhydrophilic channel (yellow part) due to the surrounding superhydrophobic confinement effect, as shown in Figure 8C (left). The superhydrophilic 3D virtual channel is further confirmed by two-photon fluorescence microscopy, as shown in Figure 8C (right). This also indicates that oxygen plasma reaches the bottom layer of the HSCPCs after 20-s etching. Moreover, proof of concept, real-time specific bioassays with high sensitivity were realized in such an optomicrofluidic system that makes post-treatment drying procedures redundant.

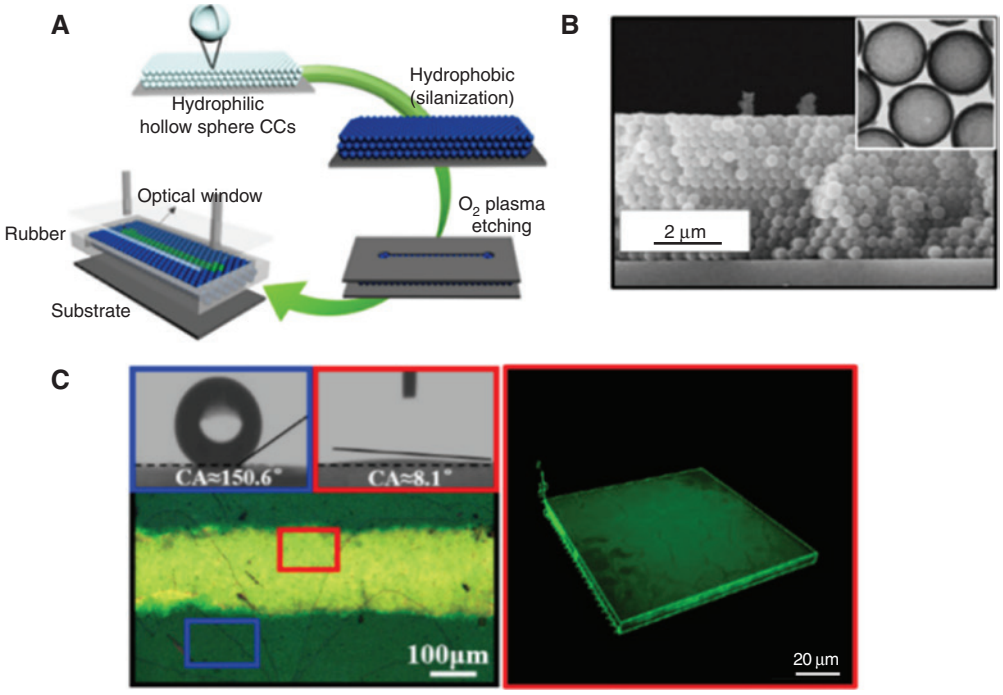

Figure 8: Fabrication of optomicrofluidics based on patterned HSCPCs.
(A) Schematic illustration of the fabrication of process. (B) A cross-section SEM image of the obtained HSCPCs, inset is a TEM image of hollow spheres. (C) Left, microscope images show the introduced superhydrophilic channel (yellow region) in the superhydrophobic HSCPCs and the corresponding contact angle measured in or out the channel, in which the invisible channel was filled with water for visualization. Right, the two-photon fluorescence image of the hydrophilic region acting as microfluidic channel. Adapted with permission from ref. [33], COPYRIGHT 2016 The Royal Society of Chemistry.

4.2.1.3 Hollow mesoporous silica spheres CPCs for selective sensing

In the past years, chemical sensing by CPCs and their derivative (inverse opal) has been realized by the shift of the reflectance spectra (PBG peak) [125, 126, 156–159]. When the solvents infiltrate into the voids of CPCs, the color of CPCs will change because the average RI of the entire CPCs is increased due to the replacement of air with solvent. However, the traditional CPC sensors cannot clearly distinguish between chemical species with similar refractive indices because of the small PBG shift. Recently, Li et al. [53] reported novel monodisperse hollow mesoporous silica spheres (HMSS) with high surface area and a narrow size distribution to assemble HMSS-CPCs, as shown in Figure 9A and B. The HMSS-CPCs show two reflection peaks, which is different from the single reflection peak of the traditional solid sphere CPCs. An interesting phenomenon was observed that remarkable PBG shifts occur for the long-wavelength reflection peak, while the short-wavelength reflection peak remains nearly constant when liquid infiltrated. Even for homologues or isomers with small RI difference, the shift of the first PBG is still significant, as shown in Figure 9C and D. The high sensitivity and selectivity of HMSS-CPCs is attributed to the hollow and mesoporous structure, which features increased specific surface and improve adsorption capabilities for the analytes.

4.2.1.4 Sealed HCPCs for ultrastable PBG and robust mechanical properties

The applications of HSCPCs mentioned above all utilize the tunable properties of the PBG of the CPCs, which are also causing the instability of the CPCs because of their inherent porosity. This means that the air among spheres of the CPCs can be readily replaced by liquid (changing the RI), which gives rise to the PBG shift. In other words, the porosity of the CPCs results in their PBG sensitive to the working environment. In addition, the porosity of the conventional CPCs also lowers their mechanical strength because there are only van der Waals interactions to connect all spheres. However, some special applications require not only an ultrastable PBG without wavelength shifting and deterioration but also robust mechanical strength. More recently, Zhong et al. [32] proposed a strategy to create sealed CPCs of hollow spheres, which is inspired by the limpet's shell. The fabrication process is shown in Figure 10A. First, TEOS precursor was introduced into the voids of the prepared PS@SiO_2 core-shell CPCs. The subsequent

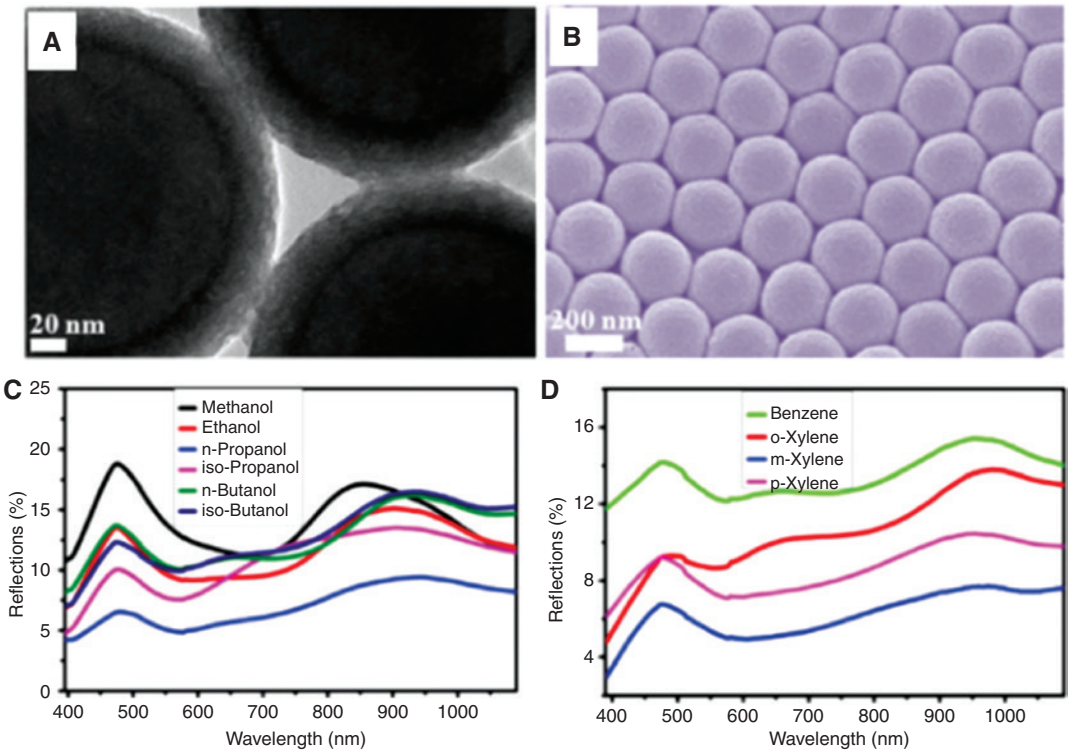

Figure 9: Self-assembled HMSS-CPCs for selective vapor sensing.
(A) A TEM image of hollow mesoporous silica spheres. (B) An SEM image of HMSS-CPCs. (C and D) Reflectance spectra of HMCPCs infiltrated with alcohol and benzene series, respectively. Adapted with permission from ref. [53], COPYRIGHT 2017 The Royal Society of Chemistry.

hydrolysis of TEOS results in the formation of silica-sealed PS@SiO_2 core-shell CPCs with an overlayer of silica. Thickness can be controlled by the spin-coating speed. Finally, removal of PS cores by calcination leads to silica-sealed hollow SiO_2 CPCs, as shown in Figure 10B. The resulting sealed CPCs show not only an ultrastable PBG under high pressure (Figure 10C) but also enhanced mechanical robustness demonstrated by a series of tests with extreme conditions, as shown in Figure 10D. Furthermore, photonic crystal lasing is achieved in such sealed HSCPCs at a constant wavelength with the sealed sample whether dry in air or submerged in water.

4.2.1.5 WGMs in hollow sphere structures

When the size of the hollow spheres matches the optical wavelength scale, it can confine and guide light along the shell of hollow spheres rather than directly pass through the shell, resulting in forming a closed light path and generating resonances at certain frequencies. This new phenomenon is generally described as a WGM, which gives rise to the coupling of incident light into particular resonant modes to enhance light trapping to substantially improve light absorption.

Cui et al. [35] have demonstrated broadband light absorption enhancement in spherical shell nanostructures due to the existence of WGM resonances. Figure 11A shows a cross-section SEM image of a monolayer of hollow spherical nanostructures. Figure 11B shows the measured absorption spectra of the sample with and without hollow spherical structures on top, in which the sample with nanostructure significantly enhances the light absorption more than the sample without hollow spherical nanostructures over a broad region. To better understand the enhancement of broadband light absorption, the authors further investigated the amplitude of the WGM electric-field patterns, as shown in Figure 11C, which corresponds to different order resonances of a single hollow sphere. These resonant modes contribute to the enhancement of broadband absorption. The absorption spectra are further broadened by optimizing the parameters of the hollow spherical structures such as size, shell thickness, and the number of layers. A similar effect has also been reported by Yin and co-workers [36], in which they employed self-assembled hollow ZnO sphere arrays to create WGM resonators to trap sunlight for improving absorption in silicon thin film solar cells. A 9.3% enhancement in the short circuit current density can be achieved theoretically by

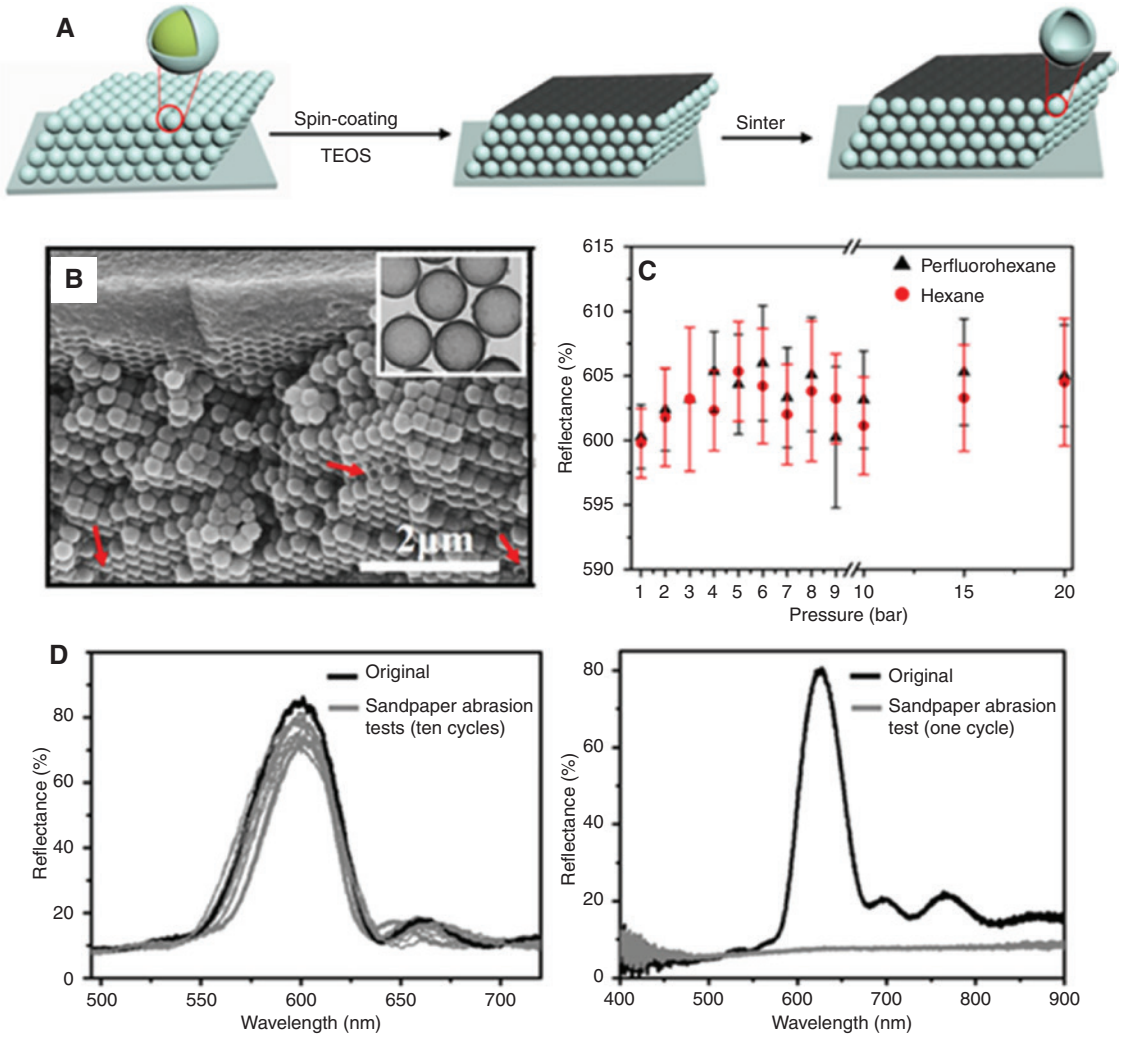

Figure 10: Fabrication of robust sealed CPCs based on hollow spheres as building blocks.
(A) Schematic illustration of the fabrication process. (B) The microscope image of the obtained sealed HSCPCs. (C) High-pressure stability of the sealed HSCPCs sample for against low surface tension liquid. (D) The comparison of mechanical strength test of the sealed HSCPCs (left) and traditional solid sphere CPCs (right) by sand paper abrasion. Adapted with permission from ref. [32], COPYRIGHT 2016 WILEY-VCH Verlag GmbH & Co. KGaA, Weinheim.

optimizing the diameter, shell thickness, and the periodicity of the hollow sphere arrays.

4.2.2 Applications of disordered assembled hollow sphere structures

4.2.2.1 Mie scattering

Compared to the (ordered) periodically self-assembled hollow sphere crystals, amorphous (disordered) ones with no positional long-range order can still significantly affect light propagation such as creating structural color and tuning the surface reflectivity. This is attributed to the unique feature of hollow spheres whose size and shape, the aspect ratio of shell thickness, and inner empty cores can fine-tune the optical properties. For instance, Armes and co-workers [160] found that their synthetic hollow sphere powders display a blue color when placed on a dark background. It was presumed that the unexpected color is attributed to a single-particle optical effect rather than their ordered close-packed structures.

Retsch et al. [51] systematically investigated the optical properties of amorphous self-assembled hollow spheres with diameter between 333 nm to 642 nm (but the shell thickness remains constant). As shown in Figure 12, the color can be tuned in a wide range. Unlike color arising from either light absorption by dyes or pigments or coherent scattering arising from long-range ordered colloidal crystals, the authors demonstrated that such colors resulted from single nanoparticle optical effect caused by

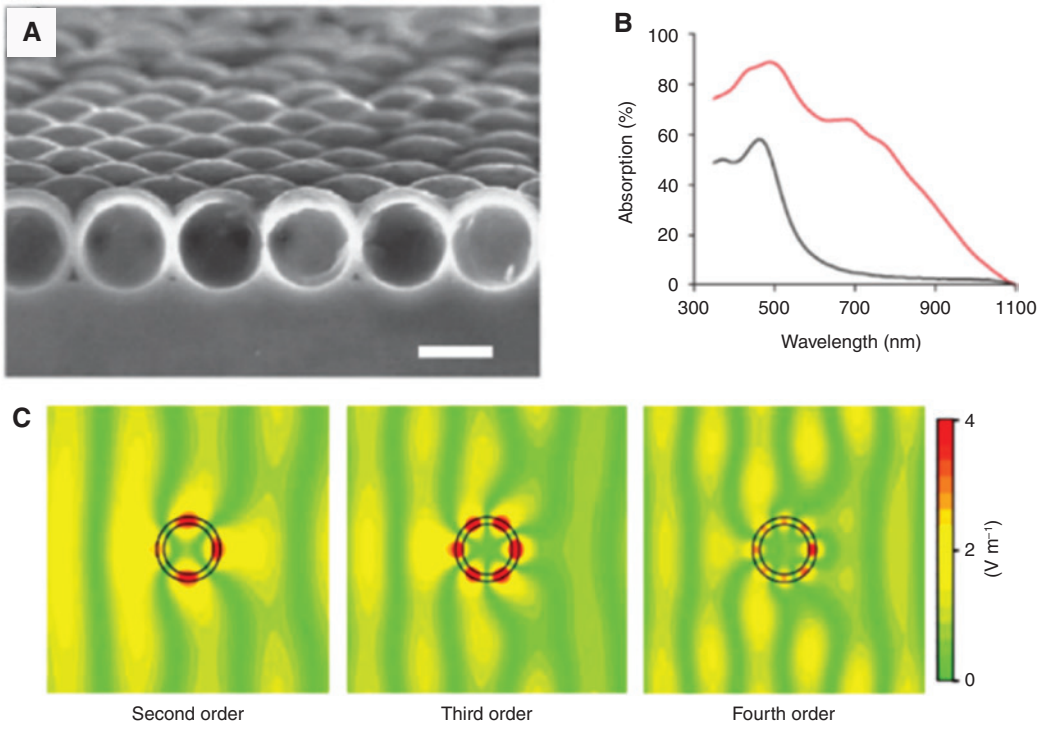

Figure 11: Light absorption enhancement based on WGMs in hollow spherical nanostructures.
(A) An SEM cross-section image of a monolayer hollow spherical structure on a substrate. (B) The comparison of absorption spectra of the sample without (black line) and with (red line) hollow spherical nanostructures measured under normally incident light with an integrating sphere. (C) Calculated electric field distribution of signal hollow spherical structure with various resonant modes. Adapted with permission from ref. [35], COPYRIGHT 2012 Macmillan Publishers Limited.

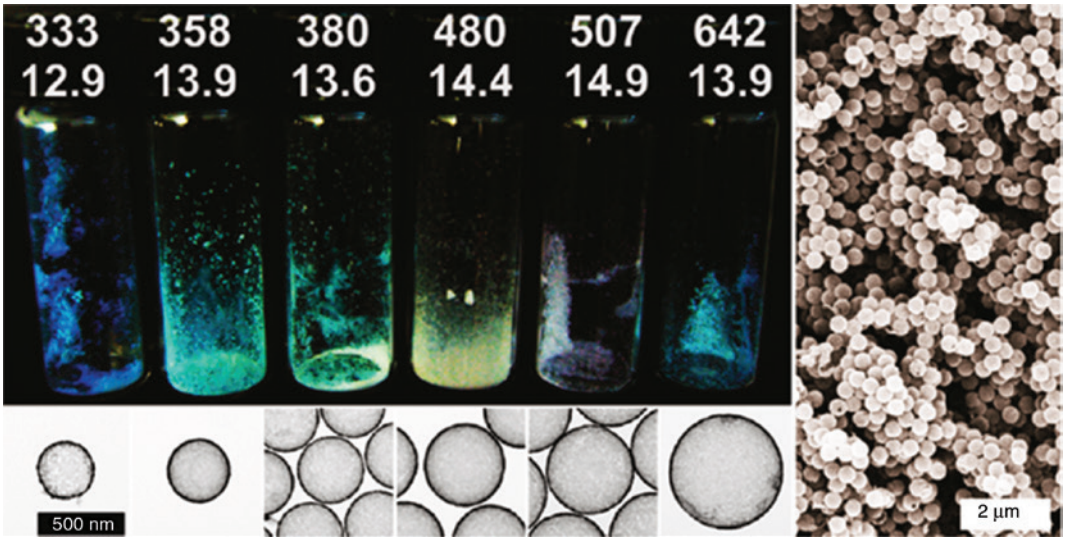

Figure 12: Amorphous powders of hollow silica spheres with various diameters displaying different colors, in which the numbers on top of the vials represent the diameter and shell thickness of hollow spheres in nanometers. The bottom panel shows the TEM images of the corresponding hollow spheres. The right panel gives an SEM image of the 380-nm amorphous powder. Adapted with permission from ref. [51], COPYRIGHT 2011 American Chemical Society.

resonant Mie scattering. The hollow silica spheres with appropriate shell thickness could dramatically increase the transport mean free path length of light, which substantially reduced background scattering. Visible Mie scattering can also be observed for fused hollow spheres with particulate shells [161]. Similar effects have also been

reported by Xu et al. for titania hollow spheres with diameter between 380 and 600 nm [162].

4.2.2.2 Antireflection coatings

Reflection is a phenomenon that occurs when light passes the interface between two media with different refractive indices. For some specific applications, surface reflectivity should be tuned such as solar reflective coating for decreasing or preventing heat radiation or antireflection coating for improving device performances. Hong et al. [163] reported the utility of hollow SiO_2 sphere as coatings to reflect solar radiations. They investigated how the size of hollow spheres and their shell structures influence solar reflectivity. It was shown that the size of the empty core of the hollow spheres has a strong impact on the reflectivity to NIR light whereas the shell itself affects the reflection of UV-blue light.

Reducing reflection has also been achieved by using hollow spheres as coatings due to the hollow feature leading to low RI. Cohen and co-workers [38] reported the utility of hollow silica spheres in fabricating conformal thin film antireflection coatings on PMMA and glass substrates. The antireflection coatings reduced the reflection of PMMA from 7% to 0.5% while it increased the transmission from 92% to 98% in the UV-visible range. Song et al. [37] reported multifunctional antireflection coatings based on hollow spheres with silica sol infiltrated. The obtained hollow sphere/silica sol composite coatings not only reduce reflection but also endow other functionalities to the substrates, including high transparency, robust resistance to moisture, high hardness, and antifogging.

5 Conclusion and perspective

Over the past two decades, hollow colloidal spheres have attracted increasing attention due to their fascinating properties and widespread classical applications in nanoreactors, photonics, drug loading and releasing, energy storage, water treatment, and so on. This review specifically highlights the recent developments of hollow spheres in NSL for directly fabricating novel nanostructures, CPCs with more advanced functionalities (e.g. lasing, optomicrofluidics, light management), and amorphous assembled nanostructures for tuning surface reflectivity. These achievements of hollow spheres are attributed to their unique features of empty cores leading to anisotropic etching, dense shell preventing liquid infiltrating resulting in remaining high RI contrast, and inside shell generating WGMs and large ratio of empty core to shell thickness for tuning the effective RI.

Although many efforts have been devoted to the synthesis of monodisperse hollow spheres with such unique properties, there is still a need for one-pot, large-scale, and low-cost synthesis routes that can meet the requirements for applications. Moreover, the toxicity for man and environment should be always a concern. In addressing these challenges, seeking new low-cost and environmental-friendly materials and better understanding of the synthesis mechanism are necessary.

Self-assembled hollow spheres provide another element for realizing these novel applications. Colloidal spheres are widely used self-assembled materials that can produce various nanostructures. These structures result in a variety of functionalities not present in the individual colloids, rendering such self-assembled colloidal spheres attractive for a range of applications, in particular, NSL, wetting, and optics. Although the past few years have witnessed a great progress in self-assembly of colloidal spheres, the preparation of large-area and highly ordered colloidal sphere arrays without defects is still a huge challenge. New methods, which can eliminate the spontaneous defects such as cracks, vacancies, dislocations, and grain boundaries, are urgently needed. Moreover, the crystalline lattice of the CCs created by the traditional self-assembly approach is very limited to the fcc structure. There are still challenges to obtain arbitrary types of crystalline lattices such as triclinic, simple cubic, and body-centered cubic lattices. This is very important towards both improving the optical properties of the CPCs (obtaining the complete PBG) and towards creating novel nanostructures.

Further research should focus on deeply understanding the current synthesis and self-assembly approaches of the hollow spheres. Better understanding these mechanisms can not only boost production of hollow spheres but also easily incorporate hollow spheres into the design and fabrication of novel functional materials and devices. We hope that a broad range of applications based on hollow spheres will emerge soon.

Acknowledgments: K. Zhong acknowledges the financial support provided by the Internal Funds KU Leuven.

References

[1] Joo JB, Zhang Q, Dahl M, et al. Synthesis, crystallinity control, and photocatalysis of nanostructured titanium dioxide shells. J Mater Res 2013;28:362–8.

[2] Kim SW, Kim M, Lee WY, et al. Fabrication of hollow palladium spheres and their successful application to the recyclable heterogeneous catalyst for suzuki coupling reactions. J Am Chem Soc 2002;124:7642–3.

[3] Sun JH, Zhang JS, Zhang MW, et al. Bioinspired hollow semiconductor nanospheres as photosynthetic nanoparticles. Nat Commun 2012;3:1139.
[4] Zhang C, Zhang R, Li X, et al. Ptni nanocrystals supported on hollow carbon spheres: enhancing the electrocatalytic performance through high-temperature annealing and electrochemical co stripping treatments. ACS Appl Mater Interfaces 2017;9:29623–32.
[5] Jeon S, Yong K. Morphology-controlled synthesis of highly adsorptive tungsten oxide nanostructures and their application to water treatment. J Mater Chem 2010;20:10146–51.
[6] Zhou X, Li X, Sun H, et al. Nanosheet-assembled znfe2o4 hollow microspheres for high-sensitive acetone sensor. ACS Appl Mater Interfaces 2015;7:15414–21.
[7] Li B, Xie Y, Jing M, et al. In_2o_3 hollow microspheres: synthesis from designed $In(OH)_3$ precursors and applications in gas sensors and photocatalysis. Langmuir 2006;22:9380–5.
[8] Cheng X, Li J, Li X, et al. A highly sensitive sensor based on hollow particles for the detection, adsorption and removal of Hg^{2+} ions. J Mater Chem 2012;22:24102–8.
[9] Wang C, Tao SY, Wei W, et al. Multifunctional mesoporous material for detection, adsorption and removal of Hg^{2+} in aqueous solution. J Mater Chem 2010;20:4635–41.
[10] Lou XW, Li CM, Archer LA. Designed synthesis of coaxial SnO_2@ Carbon hollow nanospheres for highly reversible lithium storage. Adv Mater 2009;21:2536–9.
[11] Zhang Y, Hsu BYW, Ren C, et al. Silica-based nanocapsules: synthesis, structure control and biomedical applications. Chem Soc Rev 2015;44:315–35.
[12] Lu W, Huang Q, Ku G, et al. Photoacoustic imaging of living mouse brain vasculature using hollow gold nanospheres. Biomaterials 2010;31:2617–26.
[13] Wang Q, Huang X, Long Y, et al. Hollow luminescent carbon dots for drug delivery. Carbon 2013;59:192–9.
[14] Chen Y, Xu PF, Wu MY, et al. Colloidal rbc-shaped, hydrophilic, and hollow mesoporous carbon nanocapsules for highly efficient biomedical engineering. Adv Mater 2014;26:4294–301.
[15] Chen J-F, Ding H-M, Wang J-X, et al. Preparation and characterization of porous hollow silica nanoparticles for drug delivery application. Biomaterials 2004;25:723–7.
[16] Kim H, Cho J. Template synthesis of hollow sb nanoparticles as a high-performance lithium battery anode material. Chem Mater 2008;20:1679–81.
[17] Liang HP, Zhang HM, Hu JS, et al. Pt hollow nanospheres: facile synthesis and enhanced electrocatalysts. Angew Chem Int Ed 2004;43:1540–3.
[18] Kim SM, Jeon M, Kim KW, et al. Postsynthetic functionalization of a hollow silica nanoreactor with manganese oxide-immobilized metal nanocrystals inside the cavity. J Am Chem Soc 2013;135:15714–7.
[19] Gao JS, Zhang XY, Lu Y, et al. Selective functionalization of hollow nanospheres with acid and base groups for cascade reactions. Chem Eur J 2015;21:7403–7.
[20] Perez-Lorenzo M, Vaz B, Salgueirino V, et al. Hollow-shelled nanoreactors endowed with high catalytic activity. Chem Eur J 2013;19:12196–211.
[21] Vriezema DM, Comellas Aragonès M, Elemans JAAW, et al. Self-assembled nanoreactors. Chem Rev 2005;105:1445–90.
[22] Liu J, Qiao SZ, Hartono SB, et al. Monodisperse yolk-shell nanoparticles with a hierarchical porous structure for delivery vehicles and nanoreactors. Angew Chem Int Ed 2010;49:4981–5.
[23] Yang XY, Li Y, Van Tendeloo G, et al. One-pot synthesis of catalytically stable and active nanoreactors: encapsulation of size-controlled nanoparticles within a hierarchically macroporous core@ordered mesoporous shell system. Adv Mater 2009;21:1368–72.
[24] Lee J, Kim SM, Lee IS. Functionalization of hollow nanoparticles for nanoreactor applications. Nano Today 2014;9:631–67.
[25] Pan LJ, Chortos A, Yu GH, et al. An ultra-sensitive resistive pressure sensor based on hollow-sphere microstructure induced elasticity in conducting polymer film. Nat Commun 2014;5:3002.
[26] Wang X, Feng J, Bai Y, et al. Synthesis, properties, and applications of hollow micro-/nanostructures. Chem Rev 2016;116;10983–1060.
[27] Si YS, Chen M, Wu LM. Syntheses and biomedical applications of hollow micro-/nano-spheres with large-through-holes. Chem Soc Rev 2016;45:690–714.
[28] Chen Y, Chen HR, Shi JL. Construction of homogenous/heterogeneous hollow mesoporous silica nanostructures by silica-etching chemistry: principles, synthesis, and applications. Acc Chem Res 2014;47:125–37.
[29] Lai XY, Halpert JE, Wang D. Recent advances in micro-/nano-structured hollow spheres for energy applications: from simple to complex systems. Energy Environ Sci 2012;5: 5604–18.
[30] Hu J, Chen M, Fang X, et al. Fabrication and application of inorganic hollow spheres. Chem Soc Rev 2011;40:5472–91.
[31] Nguyen CC, Vu NN, Do TO. Recent advances in the development of sunlight-driven hollow structure photocatalysts and their applications. J Mater Chem A 2015;3:18345–59.
[32] Zhong K, Liu LW, Lin JY, et al. Bioinspired robust sealed colloidal photonic crystals of hollow microspheres for excellent repellency against liquid infiltration and ultrastable photonic band gap. Adv Mater Interfaces 2016;3:1600579.
[33] Zhong K, Khorshid M, Li JQ, et al. Fabrication of optomicrofluidics for real-time bioassays based on hollow sphere colloidal photonic crystals with wettability patterns. J Mater Chem C 2016;4:7853–8.
[34] Zhong K, Wang L, Li J, et al. Real-time fluorescence detection in aqueous systems by combined and enhanced photonic and surface effects in patterned hollow sphere colloidal photonic crystals. Langmuir 2017;33:4840–6.
[35] Yao Y, Yao J, Narasimhan VK, et al. Broadband light management using low-q whispering gallery modes in spherical nanoshells. Nat Commun 2012;3:664.
[36] Yin J, Zang YS, Yue C, et al. Self-assembled hollow nanosphere arrays used as low Q whispering gallery mode resonators on thin film solar cells for light trapping. Phys Chem Chem Phys 2013;15:16874–82.
[37] Zhang X, Lan P, Lu Y, et al. Multifunctional antireflection coatings based on novel hollow silica–silica nanocomposites. ACS Appl Mater Interfaces 2014;6:1415–23.
[38] Du Y, Luna LE, Tan WS, et al. Hollow silica nanoparticles in uv–visible antireflection coatings for poly(methyl methacrylate) substrates. ACS Nano 2010;4:4308–16.
[39] Guerrero-Martinez A, Perez-Juste J, Liz-Marzan LM. Recent progress on silica coating of nanoparticles and related nanomaterials. Adv Mater 2010;22:1182–95.

[40] Zou H, Wu SS, Shen J. Polymer/silica nanocomposites: preparation, characterization, properties, and applications. Chem Rev 2008;108:3893–957.
[41] Lu Y, McLellan J, Xia YN. Synthesis and crystallization of hybrid spherical colloids composed of polystyrene cores and silica shells. Langmuir 2004;20:3464–70.
[42] Qi GG, Wang YB, Estevez L, et al. Facile and scalable synthesis of monodispersed spherical capsules with a mesoporous shell. Chem Mater 2010;22:2693–5.
[43] Hong JY, Choi M, Kim C, et al. Geometrical study of electrorheological activity with shape-controlled titania-coated silica nanomaterials. J Colloid Interface Sci 2010;347:177–82.
[44] Caruso F, Caruso RA, Mohwald H. Nanoengineering of inorganic and hybrid hollow spheres by colloidal templating. Science 1998;282:1111–4.
[45] Tissot I, Reymond JP, Lefebvre F, et al. SiOH-functionalized polystyrene latexes. A step toward the synthesis of hollow silica nanoparticles. Chem Mater 2002;14:1325–31.
[46] Sun B, Mutch SA, Lorenz RM, et al. Layered polyelectrolyte-silica coating for nanocapsules. Langmuir 2005;21:10763–9.
[47] Graf C, Vossen DLJ, Imhof A, et al. A general method to coat colloidal particles with silica. Langmuir 2003;19:6693–700.
[48] Deng TS, Marlow F. Synthesis of monodisperse polystyrene@vinyl-SiO_2 core-shell particles and hollow SiO_2 spheres. Chem Mater 2012;24:536–42.
[49] Xu XL, Asher SA. Synthesis and utilization of monodisperse hollow polymeric particles in photonic crystals. J Am Chem Soc 2004;1267940–5.
[50] Guan BY, Yu L, Li J, et al. A universal cooperative assembly-directed method for coating of mesoporous TiO_2 nanoshells with enhanced lithium storage properties. Sci Adv 2016;2:e1501554.
[51] Retsch M, Schmelzeisen M, Butt H-J, et al. Visible mie scattering in nonabsorbing hollow sphere powders. Nano Lett 2011;11:1389–94.
[52] Ruckdeschel P, Dulle M, Honold T, et al. Monodisperse hollow silica spheres: an in-depth scattering analysis. Nano Res 2016;9:1366–76.
[53] Xiong C, Zhao J, Wang L, et al. Trace detection of homologues and isomers based on hollow mesoporous silica sphere photonic crystals. Mater Horizons 2017;4:862–8.
[54] Yang J, Lind JU, Trogler WC. Synthesis of hollow silica and titania nanospheres. Chem Mater 2008;20:2875–7.
[55] Gil-Herrera LK, Blanco A, Juarez BH, et al. Seeded synthesis of monodisperse core-shell and hollow carbon spheres. Small 2016;12:4357–62.
[56] Bowen WR, Sharif AO. Long-range electrostatic attraction between like-charge spheres in a charged pore. Nature 1998;393:663–5.
[57] Kepler GM, Fraden S. Attractive potential between confined colloids at low ionic strength. Phys Rev Lett 1994;73:356–9.
[58] Larsen AE, Grier DG. Like-charge attractions in metastable colloidal crystallites. Nature 1997;385:230–3.
[59] von Freymann G, Kitaev V, Lotsch BV, et al. Bottom-up assembly of photonic crystals. Chem Soc Rev 2013;42:2528–54.
[60] Galisteo-Lopez JF, Ibisate M, Sapienza R, et al. Self-assembled photonic structures. Adv Mater 2011;23:30–69.
[61] Kruglova O, Demeyer PJ, Zhong K, et al. Wonders of colloidal assembly. Soft Matter 2013;9:9072–87.
[62] Vogel N, Retsch M, Fustin CA, et al. Advances in colloidal assembly: the design of structure and hierarchy in two and three dimensions. Chem Rev 2015;115:6265–311.
[63] Denkov ND, Velev OD, Kralchevsky PA, et al. Mechanism of formation of 2-dimensional crystals from latex-particles on substrates. Langmuir 1992;8:3183–90.
[64] Wang DY, Mohwald H. Rapid fabrication of binary colloidal crystals by stepwise spin-coating. Adv Mater 2004;16:244–7.
[65] Hayward RC, Saville DA, Aksay IA. Electrophoretic assembly of colloidal crystals with optically tunable micropatterns. Nature 2000;404:56–9.
[66] Trau M, Sankaran S, Saville DA, et al. Electric-field-induced pattern formation in colloidal dispersions. Nature 1995;374:437–9.
[67] Moon GD, Lee TI, Kim B, et al. Assembled monolayers of hydrophilic particles on water surfaces. Acs Nano 2011;5:8600–12.
[68] Zhang J-T, Wang L, Lamont DN, et al. Fabrication of large-area two-dimensional colloidal crystals. Angew Chem Int Ed 2012;51:6117–20.
[69] Fang Y, Phillips BM, Askar K, et al. Scalable bottom-up fabrication of colloidal photonic crystals and periodic plasmonic nanostructures. J Mater Chem C 2013;1:6031–47.
[70] Holgado M, Garcia-Santamaria F, Blanco A, et al. Electrophoretic deposition to control artificial opal growth. Langmuir 1999;15:4701–4.
[71] Bardosova M, Pemble ME, Povey IM, et al. The langmuir-blodgett approach to making colloidal photonic crystals from silica spheres. Adv Mater 2010;22:3104–24.
[72] Reculusa S, Ravaine S. Synthesis of colloidal crystals of controllable thickness through the langmuir-blodgett technique. Chem Mater 2003;15:598–605.
[73] Reculusa S, Massé P, Ravaine S. Three-dimensional colloidal crystals with a well-defined architecture. J Colloid Interface Sci 2004;279:471–8.
[74] Yu J, Yan QF, Shen DZ. Co-self-assembly of binary colloidal crystals at the air-water interface. ACS Appl Mater Interfaces 2010;2:1922–6.
[75] Vogel N, de Viguerie L, Jonas U, et al. Wafer-scale fabrication of ordered binary colloidal monolayers with adjustable stoichiometries. Adv Funct Mater 2011;21:3064–73.
[76] Woodcock LV. Entropy difference between the face-centred cubic and hexagonal close-packed crystal structures. Nature 1997;385:141–3.
[77] Xia YN, Gates B, Yin YD, et al. Monodispersed colloidal spheres: old materials with new applications. Adv Mater 2000;12:693–713.
[78] Marlow F, Muldarisnur, Sharifi P, et al. Opals: status and prospects. Angew Chem Int Ed 2009;48:6212–33.
[79] Jiang P, Bertone JF, Hwang KS, et al. Single-crystal colloidal multilayers of controlled thickness. Chem Mater 1999;11:2132–40.
[80] Wong S, Kitaev V, Ozin GA. Colloidal crystal films: advances in universality and perfection. J Am Chem Sci 2003;125:15589–98.
[81] Steele A, Bayer I, Loth E. Inherently superoleophobic nanocomposite coatings by spray atomization. Nano Lett 2009;9:501–5.
[82] Campos R, Guenthner AJ, Meuler AJ, et al. Superoleophobic surfaces through control of sprayed-on stochastic topography. Langmuir 2012;28:9834–41.

[83] Cebeci FÇ, Wu Z, Zhai L, et al. Nanoporosity-driven superhydrophilicity: a means to create multifunctional antifogging coatings. Langmuir 2006;22:2856–62.
[84] Bravo J, Zhai L, Wu Z, et al. Transparent superhydrophobic films based on silica nanoparticles. Langmuir 2007;23:7293–8.
[85] Hulteen JC, Vanduyne RP. Nanosphere lithography: a materials general fabrication process for periodic particle array surfaces. J Vac Sci Technol 1995;13:1553–8.
[86] Zhang JH, Li YF, Zhang XM, et al. Colloidal self-assembly meets nanofabrication: from two-dimensional colloidal crystals to nanostructure arrays. Adv Mater 2010;22:4249–69.
[87] Yang SM, Jang SG, Choi DG, et al. Nanomachining by colloidal lithography. Small 2006;2:458–75.
[88] Colson P, Henrist C, Cloots R. Nanosphere lithography: a powerful method for the controlled manufacturing of nanomaterials. J Nanomater 2013;2013:948510.
[89] Zhang XY, Whitney AV, Zhao J, et al. Advances in contemporary nanosphere lithographic techniques. J Nanosci Nanotechnol 2006;6:1920–34.
[90] Haynes CL, Van Duyne RP. Nanosphere lithography: a versatile nanofabrication tool for studies of size-dependent nanoparticle optics. J Phys Chem B 2001;105:5599–611.
[91] Saavedra HM, Mullen TJ, Zhang PP, et al. Hybrid strategies in nanolithography. Rep Prog Phys 2010;73:036501–40.
[92] Lu Y, Liu GL, Kim J, et al. Nanophotonic crescent moon structures with sharp edge for ultrasensitive biomolecular detection by local electromagnetic field enhancement effect. Nano Lett 2005;5:119–24.
[93] Choi DG, Yu HK, Jang SG, et al. Colloidal lithographic nanopatterning via reactive ion etching. J Am Chem Sci 2004;126:7019–25.
[94] Vinckx W, Vanacken J, Moshchalkov VV. Vortex pinning in nb thin films modulated by nanospheres. J Appl Phys 2006;100:7.
[95] Ye X, Li Y, Dong J, et al. Facile synthesis of zns nanobowl arrays and their applications as 2d photonic crystal sensors. J Mater Chem C 2013;1:6112–9.
[96] Ren ZY, Zhang XM, Zhang JJ, et al. Building cavities in microspheres and nanospheres. Nanotechnology 2009;20:065305.
[97] Ye J, Verellen N, Van Roy W, et al. Plasmonic modes of metallic semishells in a polymer film. ACS Nano 2010;4:1457–64.
[98] Cai YJ, Li Y, Nordlander P, et al. Fabrication of elliptical nanorings with highly tunable and multiple plasmonic resonances. Nano Lett 2012;12:4881–8.
[99] Chen JX, Liao WS, Chen X, et al. Evaporation-induced assembly of quantum dots into nanorings. ACS Nano 2009;3:173–80.
[100] Halpern AR, Corn RM. Lithographically patterned electrodeposition of gold, silver, and nickel nanoring arrays with widely tunable near-infrared plasmonic resonances. ACS Nano 2013;7:1755–62.
[101] Cheung CL, Nikolic RJ, Reinhardt CE, et al. Fabrication of nanopillars by nanosphere lithography. Nanotechnology 2006;17:1339–43.
[102] Min WL, Jiang B, Jiang P. Bioinspired self-cleaning antireflection coatings. Adv Mater 2008;20:3914–8.
[103] Hall AS, Friesen SA, Mallouk TE. Wafer-scale fabrication of plasrnonic crystals from patterned silicon templates prepared by nanosphere lithography. Nano Lett 2013;13:2623–7.
[104] Nemiroski A, Gonidec M, Fox JM, et al. Engineering shadows to fabricate optical metasurfaces. ACS Nano 2014;8:11061–70.
[105] Chen K, Rajeeva BB, Wu ZL, et al. Moire nanosphere lithography. ACS Nano 2015;9:6031–40.
[106] Zhao Z, Cao Y, Cai YJ, et al. Oblique colloidal lithography for the fabrication of nonconcentric features. ACS Nano 2017;11:6594–604.
[107] Kim DS, Park MS, Jang JH. Fabrication of cone-shaped subwavelength structures by utilizing a confined convective self-assembly technique and inductively coupled-plasma reactive-ion etching. J Vac Sci Technol B 2011;29:5.
[108] Zhong K, Li J, Liu L, et al. Direct fabrication of monodisperse silica nanorings from hollow spheres–a template for core-shell nanorings. ACS Appl Mater Interfaces 2016;8:10451–8.
[109] Zhong K, Demeyer PJ, Zhou X, et al. A facile way to introduce planar defects into colloidal photonic crystals for pronounced passbands. J Mater Chem C 2014;2:8829–36.
[110] Zhong K, Li JQ, Van Cleuvenbergen S, et al. Direct fabrication of complex 3d hierarchical nanostructures by reactive ion etching of hollow sphere colloidal crystals. Nanoscale 2016;8:15845–9.
[111] Tan BJY, Sow CH, Lim KY, et al. Fabrication of a two-dimensional periodic non-close-packed array of polystyrene particles. J Phys Chem B 2004;108:18575–9.
[112] Deng T, Cournoyer JR, Schermerhorn JH, et al. Generation and assembly of spheroid-like particles. J Am Chem Soc 2008;130:14396–7.
[113] von Freymann G, John S, Kitaev V, et al. Enhanced coupling to slow photon modes in three-dimensional graded colloidal photonic crystals. Adv Mater 2005;17:1273–6.
[114] Grandidier J, Callahan DM, Munday JN, et al. Light absorption enhancement in thin-film solar cells using whispering gallery modes in dielectric nanospheres. Adv Mater 2011;23:1272.
[115] Gonzalez-Urbina L, Baert K, Kolaric B, et al. Linear and nonlinear optical properties of colloidal photonic crystals. Chem Rev 2012;112:2268–85.
[116] Gottardo S, Sapienza R, Garcia PD, et al. Resonance-driven random lasing. Nat Photonics 2008;2:429–32.
[117] Cerdán L, Costela A, Enciso E, et al. Random lasing in self-assembled dye-doped latex nanoparticles: Packing density effects. Adv Funct Mater 2013;23:3916–24.
[118] Anderson PW. Absence of diffusion in certain random lattices. Phys Rev 1958;109:1492–505.
[119] Buskens P, Burghoorn M, Mourad MCD, et al. Antireflective coatings for glass and transparent polymers. Langmuir 2016;32:6781–93.
[120] Lopez C. Materials aspects of photonic crystals. Adv Mater 2003;15:1679–704.
[121] Lodahl P, van Driel AF, Nikolaev IS, et al. Controlling the dynamics of spontaneous emission from quantum dots by photonic crystals. Nature 2004;430:654–7.
[122] Furumi S. Recent advances in polymer colloidal crystal lasers. Nanoscale 2012;4:5564–71.
[123] Furumi S. Self-assembled organic and polymer photonic crystals for laser applications. Polym J 2013;45:579–93.
[124] Rinne SA, Garcia-Santamaria F, Braun PV. Embedded cavities and waveguides in three-dimensional silicon photonic crystals. Nat Photonics 2008;2:52–6.
[125] Fenzl C, Hirsch T, Wolfbeis OS. Photonic crystals for chemical sensing and biosensing. Angew Chem Int Ed 2014;53:3318–35.
[126] Ge J, Yin Y. Responsive photonic crystals. Angew Chem Int Ed 2011;50:1492–522.
[127] Stober W, Fink A, Bohn E. Controlled growth of monodisperse silica spheres in the micron size range. J Colloid Interface Sci 1968;26:62–9.

[128] Liu ZF, Ding T, Zhang G, et al. Ternary inverse opal system for convenient and reversible photonic bandgap tuning. Langmuir 2008;24:10519–23.
[129] Yablonovitch E, Gmitter TJ, Meade RD, et al. Donor and acceptor modes in photonic band structure. Phys Rev Lett 1991;67:3380–3.
[130] Pradhan RD, Tarhan İİ, Watson GH. Impurity modes in the optical stop bands of doped colloidal crystals. Phys Rev B 1996;54:13721–6.
[131] Yan Q, Wang L, Zhao XS. Artificial defect engineering in three-dimensional colloidal photonic crystals. Adv Funct Mater 2007;17:3695–706.
[132] Braun PV, Rinne SA, Garcia-Santamaria F. Introducing defects in 3D photonic crystals: state of the art. Adv Mater 2006;18:2665–78.
[133] Zhao YX, Wostyn K, de Schaetzen G, et al. The fabrication of photonic band gap materials with a two-dimensional defect. Appl Phys Lett 2003;82:3764–6.
[134] Wostyn K, Zhao YX, de Schaetzen G, et al. Insertion of a two-dimensional cavity into a self-assembled colloidal crystal. Langmuir 2003;19:4465–8.
[135] Dechezelles J-F, Masse P, Cloutet E, et al. Building planar defects into colloidal crystals using particles of different chemical nature. Colloids Surf A Physicochem Eng Asp 2009;343:8–11.
[136] Masse P, Vallee RAL, Dechezelles J-F, et al. Effects of the position of a chemically or size-induced planar defect on the optical properties of colloidal crystals. J Phys Chem C 2009;113:14487–92.
[137] Palacios-Lidon E, Galisteo-Lopez JF, Juarez BH, et al. Engineered planar defects embedded in opals. Adv Mater 2004;16:341–5.
[138] Tetreault N, Mihi A, Miguez H, et al. Dielectric planar defects in colloidal photonic crystal films. Adv Mater 2004;16:346–9.
[139] Pozas R, Mihi A, Ocana M, et al. Building nanocrystalline planar defects within self-assembled photonic crystals by spin-coating. Adv Mater 2006;18:1183–7.
[140] Fleischhaker F, Arsenault AC, Peiris FC, et al. DNA designer defects in photonic crystals: optically monitored biochemistry. Adv Mater 2006;18:2387–91.
[141] Tetreault N, Arsenault AC, Mihi A, et al. Building tunable planar defects into photonic crystals using polyelectrolyte multilayers. Adv Mater 2005;17:1912–6.
[142] Fleischhaker F, Arsenault AC, Kitaev V, et al. Photochemically and thermally tunable planar defects in colloidal photonic crystals. J Am Chem Soc 2005;127:9318–9.
[143] Phan Ngoc H, Benalloul P, Coolen L, et al. A sputtered-silica defect layer between two artificial silica opals: an efficient way to engineer well-ordered sandwich structures. J Mater Chem C 2013;1:5381–6.
[144] Dokukin ME, Baryshev AV, Khanikaev AB, et al. Reverse and enhanced magneto-optics of opal-garnet heterostructures. Opt Express 2009;17:9062–70.
[145] Noda S, Yokoyama M, Imada M, et al. Polarization mode control of two-dimensional photonic crystal laser by unit cell structure design. Science 2001;293:1123–5.
[146] Painter O, Lee RK, Scherer A, et al. Two-dimensional photonic band-gap defect mode laser. Science 1999;284:1819–21.
[147] Park HG, Kim SH, Kwon SH, et al. Electrically driven single-cell photonic crystal laser. Science 2004;305:1444–7.
[148] Furumi S. Active lasing from organic colloidal photonic crystals. J Mater Chem C 2013;1:6003–12.
[149] Zhong K, Liu LW, Xu XD, et al. Defect mode passband lasing in self-assembled photonic crystal. ACS Photonics 2016;3:2330–7.
[150] Yan YY, Gao N, Barthlott W. Mimicking natural superhydrophobic surfaces and grasping the wetting process: a review on recent progress in preparing superhydrophobic surfaces. Adv Colloid Interface Sci 2011;169:80–105.
[151] Wang JX, Zhang YZ, Wang ST, et al. Bioinspired colloidal photonic crystals with controllable wettability. Acc Chem Res 2011;44:405–15.
[152] Sato O, Kubo S, Gu Z-Z. Structural color films with lotus effects, superhydrophilicity, and tunable stop-bands. Acc Chem Res 2009;42:1–10.
[153] Burgess IB, Loncar M, Aizenberg J. Structural colour in colourimetric sensors and indicators. J Mater Chem C 2013;1:6075–86.
[154] Hou J, Zhang HC, Yang Q, et al. Bio-inspired photonic-crystal microchip for fluorescent ultratrace detection. Angew Chem Int Ed 2014;53:5791–5.
[155] Parker AR, Lawrence CR. Water capture by a desert beetle. Nature 2001;414:33–4.
[156] Xu H, Wu P, Zhu C, et al. Photonic crystal for gas sensing. J Mater Chem C 2013;1:6087–98.
[157] Aguirre CI, Reguera E, Stein A. Tunable colors in opals and inverse opal photonic crystals. Adv Funct Mater 2010;20:2565–78.
[158] Zhao Y, Xie Z, Gu H, et al. Bio-inspired variable structural color materials. Chem Soc Rev 2012;41:3297–317.
[159] NU Department of Molecular Design and Engineering, Furocho, Chikusa-ku, Nagoya. Structural colored gels for tunable soft photonic crystals. Chem Rec 2009;9:87–105.
[160] Schmid A, Fujii S, Armes SP, et al. Polystyrene – silica colloidal nanocomposite particles prepared by alcoholic dispersion polymerization. Chem Mater 2007;19:2435–45.
[161] Fielding LA, Mykhaylyk OO, Schmid A, et al. Visible mie scattering from hollow silica particles with particulate shells. Chem Mater 2014;26:1270–7.
[162] Xu H, Chen X, Ouyang S, et al. Size-dependent Mie's scattering effect on TiO_2 spheres for the superior photoactivity of H_2 evolution. J Phys Chem C 2012;116:3833–9.
[163] Xing Z, Tay S-W, Ng YH, et al. Porous SiO_2 hollow spheres as a solar reflective pigment for coatings. ACS Appl Mater Interfaces 2017;9:15103–13.